The myelin content of the human precentral hand knob reflects inter-individual differences in manual motor control at the physiological and behavioural level

Dubbioso, Raffaele; Madsen, Kristoffer Hougaard; Thielscher, Axel; Siebner, Hartwig Roman

Published in:
Journal of neuroscience

Link to article, DOI:
10.1523/JNEUROSCI.0390-20.2021

Publication date:
2021

Document Version
Peer reviewed version

JNeurosci
THE JOURNAL OF NEUROSCIENCE

Research Articles: Systems/Circuits

The myelin content of the human precentral hand knob reflects inter-individual differences in manual motor control at the physiological and behavioural level

https://doi.org/10.1523/JNEUROSCI.0390-20.2021

Cite as: J. Neurosci 2021; 10.1523/JNEUROSCI.0390-20.2021

Received: 18 February 2020
Revised: 22 February 2021
Accepted: 24 February 2021

The myelin content of the human precentral hand knob reflects inter-individual differences in manual motor control at the physiological and behavioural level

Raffaele Dubbioso[1,2*], Kristoffer Hougaard Madsen[1,3], Axel Thielscher[1,4], Hartwig Roman Siebner[1,5,6*]

[1]Danish Research Centre for Magnetic Resonance, Centre for Functional and Diagnostic Imaging and Research, Copenhagen University Hospital Hvidovre, Hvidovre, Denmark

[2]Department of Neurosciences, Reproductive Sciences and Odontostomatology, University Federico II of Naples, Naples, Italy.

[3]Department of Applied Mathematics and Computer Science, Technical University of Denmark, Kgs. Lyngby, Denmark.

[4]Department of Health Technology, Technical University of Denmark, Kgs. Lyngby, Denmark.

[5]Department of Neurology, Copenhagen University Hospital Bispebjerg, Copenhagen, Denmark.

[6]Institute for Clinical Medicine, Faculty of Health and Medical Sciences, University of Copenhagen, Copenhagen, Denmark

Short title: Structure-function relationships in the precentral motor hand knob

Word count: Abstract: 250; Introduction: 759; Discussion: 2864

Number of figures: 7; **Tables:** 1

***Corresponding authors**

Raffaele Dubbioso, MD, PhD
Department of Neurosciences, Reproductive Sciences and Odontostomatology, University Federico II of Napoli, Via Sergio Pansini, 5. 80131 Napoli, Italy.
Phone: +39 0817464579. e-mail: rafdubbioso@gmail.com
Hartwig R. Siebner, MD, DMSc
Danish Research Centre for Magnetic Resonance (DRCMR), Center for Functional and Diagnostic Imaging and Research, Copenhagen University Hospital Hvidovre, Kettegård Allé 30, DK-2650 Hvidovre, Denmark.
Phone: +45 3862 6541 -, e-mail: h.siebner@drcmr.dk

Acknowledgments

We thank Sofie Johanna Nilsson for helping with the acquisition of MRI data. We are grateful to Lasse Christiansen, Peter Jagd Sørensen, Silas Haahr Nielsen, Estelle Raffin and Johannes Stelzer for data analysis and comments on the manuscript. We would like to thank Antoine Lutti, Gunther Helms, and Nikolas Weiskopf for providing the multiparameter MRI sequence which was used to obtain quantitative R1 maps.

Author Contributions

R.D. designed the study, acquired, pre-processed, analysed and interpreted the data, and drafted a first version of the manuscript.

K.H.M. designed the study, participated in analysis and interpretation of the data

A.T. designed the study, participated in analysis and interpretation of the data

H.R.S. designed the study, participated in interpretation of the data and in drafting a first version of the manuscript.

Conflict of Interest

Hartwig R. Siebner has received honoraria as speaker from Sanofi Genzyme, Denmark and Novartis, Denmark, as consultant from Sanofi Genzyme, Denmark and Lundbeck AS, Denmark, and as editor-in-chief (Neuroimage Clinical) and senior editor (NeuroImage) from Elsevier Publishers, Amsterdam, The Netherlands. He has received royalties as book editor from Springer Publishers, Stuttgart, Germany and from Gyldendal Publishers, Copenhagen, Denmark. The other authors report no conflict of interests.

Funding

This work is part of the project “Biophysically adjusted state-informed cortex stimulation” (BASICS) funded by a synergy grant from Novo Nordisk Foundation (Interdisciplinary Synergy Program 2014; grant number NNF14OC001. Hartwig R. Siebner holds a 5-year professorship in precision medicine at the Faculty of Health Sciences and Medicine, University of Copenhagen which is sponsored by the Lundbeck Foundation (Grant Nr. R186-2015-2138).

Abstract

The primary motor hand area ($M1_{HAND}$) and adjacent dorsal premotor cortex (PMd) form the so-called motor hand knob in the precentral gyrus. $M1_{HAND}$ and PMd are critical for dexterous hand use and are densely inter-connected via cortico-cortical axons, lacking a sharp demarcating border. In 24 young right-handed volunteers, we performed multi-modal mapping to delineate the relationship between structure and function in the right motor hand knob. Quantitative structural magnetic resonance imaging (MRI) at 3 Tesla yielded regional R1-maps as a proxy of cortical myelin content. Participants also underwent functional MRI. We mapped task-related activation and temporal precision, while they performed a visuo-motor synchronization task requiring visually cued abduction movements with the left index or little finger. We also performed sulcus-aligned transcranial magnetic stimulation (TMS) of the motor hand knob to localize the optimal site (hotspot) for evoking a motor evoked potential (MEP) in two intrinsic hand muscle. Individual motor hotspot locations varied along the rostro-caudal axis. The more rostral the motor hotspot location in the precentral crown, the longer were corticomotor MEP latencies. "Hotspot rostrality" was associated with the regional myelin content in the precentral hand knob. Cortical myelin content also correlated positively with task-related activation of the precentral crown and temporal precision during the visuo-motor synchronization task. Together, our results suggest a link between cortical myelination, the spatial cortical representation and temporal precision of finger movements. We hypothesize that the myelination of cortical axons facilitates neuronal integration in PMd and $M1_{HAND}$ and hereby, promotes the precise timing of movements.

Significance statement

Here we used magnetic resonance imaging and transcranial magnetic stimulation (TMS) of the precentral motor hand knob to test for a link between cortical myelin content, functional cortico-motor representations, and manual motor control. A higher myelin content of the precentral motor hand knob was associated with more rostral corticomotor presentations, with stronger task-related activation and a higher precision of movement timing during a visuo-motor synchronization task. We propose that a high precentral myelin content enables fast and precise neuronal integration in M1 and PMd, resulting in higher temporal precision during dexterous hand use. Our results identify the degree of myelination as an important structural feature of the neocortex that is tightly linked to the function and behaviour supported by the cortical area.

Keywords: motor skill, premotor cortex, primary motor cortex, functional cortical mapping, magnetic resonance imaging.

Introduction

The primary motor hand area ($M1_{HAND}$) and adjacent dorsal premotor cortex (PMd) are critical for dexterous hand use in human and non-human primates. The $M1_{HAND}$ enables the independent use of single fingers through direct cortico-motoneuronal control of hand and finger muscles (Lemon, 2008, 2019). The rostral ("old") and caudal ("new") parts of $M1_{HAND}$ differ with respect to their cortico-motoneuronal connectivity (Rathelot and Strick, 2006, 2009; Witham et al., 2016). Only the caudal $M1_{HAND}$ which is located deep in the anterior wall of the precentral sulcus contains large, fast-conducting pyramidal cells that produce short-latency monosynaptic responses in spinal motoneurons. The rostral part of $M1_{HAND}$ (and the somatosensory area 3a) exert descending motor control over cervical spinal motoneurons via more slowly conducting monosynaptic as well as di-synaptic projections (Witham et al., 2016). The PMd also plays an important role in manual motor control, contributing to the selection and execution of hand and finger movements (Picard and Strick, 2001; Ward et al., 2010). Its prominent role is reflected by dense reciprocal connections with $M1_{HAND}$ (Dum and Strick, 2005) and by the fact that the most caudal part of PMd contains scattered large pyramidal cells which send axonal projections to the cervical cord via the pyramidal tract (Geyer et al., 2000).

The $M1_{HAND}$ and PMd form a characteristic knob-like structure in the human precentral gyrus (Yousry et al., 1997). The precentral motor hand knob can be easily identified by structural magnetic resonance imaging (MRI) due to its visible omega or epsilon shape (Yousry et al., 1997). The $M1_{HAND}$ and PMd lack a clear anatomical demarcation line. Cytoarchitectonic mapping studies showed that the rostral border of the primary motor cortex extends to the surface of the precentral crown close to the midline, but retracts to the rostral bank of the central sulcus in more lateral parts of the hemisphere (Geyer et al., 1996, 2000). The caudal PMd occupies most of the crown and lip of the precentral hand region and belongs cyto-architectonically to Brodmann area 6 (BA6). However, the transition between rostral $M1_{HAND}$ and caudal PMd is smooth and there is subject inter-individual variability regarding the rostral extension of the $M1_{HAND}$ (Geyer et al., 1996, 2000). In agreement with a smooth cytoarchitectonic transition, the dendritic tree of supragranular (layer III) pyramidal cells in the precentral cortex of macaques becomes gradually more complex with rostral progression from the central sulcus (M1) to adjacent premotor cortex (Elston and Rockland, 2002).

The physiology of the precentral motor hand knob and its corticomotor output to the contralateral hand can be studied in humans with transcranial magnetic stimulation (TMS) (Barker et al., 1985; Palmer and Ashby, 1992; Maertens De Noordhout et al., 1999; Groppa et al., 2012). The site to target $M1_{HAND}$ is functionally defined as the site where TMS elicits the largest motor evoked potential (MEP) in contralateral hand muscles, commonly referred to as "motor hotspot" (Groppa et al., 2012; Rossini et al., 2015). But TMS can also be used to map the functional topography of corticomotor representations by applying TMS at different scalp positions using a two-dimensional grid (Wassermann et al., 1993; Pascual-Leone et al., 1994; Veldema et al., 2017). TMS-based corticomotor mapping has consistently shown substantial inter-individual variations in precentral motor hotspot location along the anterior-posterior grid axis (Teitti et al., 2008; Diekhoff et al., 2011; Vaalto et al., 2011; Sarfeld et al., 2012; Ahdab et al., 2014, 2016).

Post-mortem myeloarchitectonic analyses have shown that the precentral gyrus is one of the cortical areas which contains the highest density of myelinated axons (Nieuwenhuys, 2013). Using myelin-sensitive read-outs (Glasser and van Essen, 2011; Lutti et al., 2014), in vivo magnetic resonance imaging (MRI) confirmed that the myelin content in the frontal cortex peaks in the pericentral gyrus and then gradually decreases along a posterior-anterior gradient (Glasser and van Essen, 2011). MRI-based cortical myelin mapping also revealed considerable inter-individual variability (Shams et al., 2019) with respect to the regional myelin content. Since myelination enables fast signal propagation and synchronizes neural activity (Seidl et al., 2010; Pajevic et al., 2014; Ford et al., 2015; Timmler and Simons, 2019), the degree of precentral myelination may account for functional phenotypic variation in precentral cortical function and dexterous hand use. To test this hypothesis, we combined structural myelin-sensitive MRI, task-related functional MRI, with a novel sulcus-aligned TMS mapping approach. We reasoned that our multimodal mapping approach can reveal structural and functional features in the precentral gyrus that may account for inter-individual variability regarding the evoked corticomotor responses and contribute to inter-individual differences in the plasticity-inducing effects of repetitive TMS on corticomotor excitability.

Materials and methods

Participants and power analysis

Our main goal was to detect a link between regional cortical myelination and a read-out of corticomotor representation as revealed by our novel TMS mapping procedure (see below for details). Since this novel TMS-based measure (i.e., rostrality index) had not been used in previous work, we could not perform a proper power analysis. We therefore based our sample size estimation on previous neurophysiological TMS mapping studies. Here, the number of participants included in a single study ranged from 11 to 17 healthy volunteers (Teitti et al., 2008; Diekhoff et al., 2011; Vaalto et al., 2011, 2016; Sarfeld et al., 2012; Ahdab et al., 2014, 2016). We decided to recruit 24 participants to secure a sample size that exceeded previous TMS mapping studies, factoring in an estimated drop-out rate of 20%.

Twenty-four healthy young adults (12 women and 12 men) with a mean age of 24 years, ranging from 19 to 34 years, and a mean height of 173 cm (range: 163-187 cm) participated in this study. Participants were consistently right-handed as assessed by the Edinburgh handedness inventory (Oldfield, 1971). Only individuals with little (<2 years) or no formal music training were included. They had no previous history of neurological or psychiatric disorders and were screened for contraindications to TMS (Rossi et al., 2009). They all gave written informed consent to the experimental procedures. The study complied with the Helsinki declaration on human experimentation and was approved by the Ethical Committee of the Capital Region of Denmark (H-15000551).

Experimental procedures and data acquisition

Experimental procedures are illustrated in Fig.1 and comprise corticomotor TMS mapping as well as structural and functional magnetic resonance (MRI) of the whole brain at 3 tesla. All participants underwent structural and functional MRI the day before the TMS mapping experiment. All MRI scans were acquired with a 3 T Verio Scanner and a 32-channel head coil (Siemens, Erlangen, Germany).

Structural MRI

Structural T1-weighted images were acquired to assess cortical thickness and to individually identify and track the TMS-target points with frameless stereotactic neuronavigation on each participant's macrostructure. The T1-weighted images had an isotropic resolution with a voxel size of $1mm^3$ (TR = 2300

ms, TE = 2.96 ms, flip angle = 9°). T2-weighted images were acquired to inform offline simulation of the induced electric fields in the precentral gyrus in each individual participant given the intensity of the stimulation and the distance of the coil from the scalp in each condition. T2-weighted whole-brain scans had a voxel size of 1x1x2 mm^3 (TR = 10000ms, TE = 52ms, flip angle= 120˚). In addition, a whole-brain multiparameter mapping protocol was run to obtain quantitative R1 maps as an index of regional cortical myelination (Helms et al., 2008; Lutti et al., 2010). The protocol is based on multi-echo 3D Proton Density- and T1-weighted FLASH (fast low angle shot) images at 1 mm isotropic resolution, which undergo correction for radio frequency (RF) transmit field inhomogeneities using an EPI (echo-planar imaging)-based B1+ map. The latter is corrected for off-resonance effects using a B0 field map. For further details regarding the sequence parameters, we refer to two publications (Weiskopf and Helms, 2008; Weiskopf et al., 2011).

Functional MRI

Functional MRI used a gradient-echo planar imaging (EPI) sequence sensitive to detect task-related blood-oxygenation level dependent (BOLD) changes in tissue contrast (TR = 2.07 s, TE = 30 ms, flip angle = 78°, voxel size = 2×2×2 mm^3, axial field of view = 192×192 mm). A single brain volume consisted of 25 axial slices covering the upper half of the brain. The axial orientation of the brain volumes orientation was slightly tilted backwards so that the orientation of the slices was approximately perpendicular to the course of the central sulcus. 335 brain volumes were acquired during the fMRI session. Two additional short whole-brain EPI scans (62 slices) with the same parameters except for an adjusted TR were recorded for co-registration purposes. Pulse and respiration were recorded with an infrared pulse oximeter and a pneumatic thoracic belt.

Task related activity changes were mapped with BOLD fMRI while participants performed a repetitive isometric finger abduction task with their left index or little finger (Fig.1D). This task engaged the same muscles that were investigated with TMS, namely the FDI and ADM muscle. The left hand of the subject was placed on a board fitted with two strain gauge sensors measuring the abduction forces produced with the index or little finger (Fig.1D). The strain gauges sensors were connected to a custom amplifier which converted the measured force to a voltage in the range 0-2.5 V, this signal was sampled via a PicoLog 1216 USB 2.0 acquisition device at a sampling rate of 500 Hz. Involuntary movement of the thumb, the middle and the ring finger were avoided by using adhesive felt. Subjects saw a schematic drawing of the back of the

left hand displayed on a video screen that was visible to the subjects via a coil-mounted mirror. Red or green dots were presented every second at the tip of the left index or little finger. Participants had to produce an isometric abduction with the corresponding finger, whenever a green dot appeared at the tip of the target finger. Participants had to refrain from any movement, whenever a red dot was presented. Using a block design, the same dot and colour was presented 10 times. The duration of presentation of green or red dots within each block was 0.5 s at a constant frequency of 1 Hz without any jitter. The visuo-motor synchronization task consisted of blocks of movements (green dots) alternated with blocks without movements (red dots). The four task conditions were always performed in a fixed order and repeated 18 times during the fMRI run (Fig.1D). Stimulus presentation and response recording was controlled by custom-made programs (PsychoPy software, v. 1.74.01, www.psychopy.org) (Peirce, 2009). Immediately before the fMRI experiment, all participants performed a short training version of the task outside the MRI scanner to get familiarized with the task. We instructed participants to emphasize on the timing of movement and try to synchronize as best as possible movement rate to the pace of the visual cue to the best of their ability. Performance of the subjects in the scanner was controlled by video monitoring. Importantly, we were interested in movement regularity and synchronization to visual inputs, rather than in the accuracy of responding with the correct finger or producing a constant abduction force. Therefore, our task probed visuo-to-motor synchronization of simple repetitive finger movements rather than visuo-to-motor response mapping. We reasoned that the degree of cortical myelination in the precentral hand knob should scale with temporal precision of movement (i.e., the ability to reliably adjust movement repetition rate to the pace of the external cue). Therefore, we hypothesized that high levels of precentral cortical myelination should be associated with low trial-to-trial variability of the between-movement interval during the visually cued movement synchronization task.

Transcranial magnetic stimulation

We applied a sulcus-aligned TMS mapping approach that has been developed by our group (Raffin et al., 2015; Dubbioso et al., 2017; Raffin and Siebner, 2018) to precisely localize the optimal site for evoking MEPs in two intrinsic hand muscles (i.e., precentral motor hotspot) along the rostro-caudal axis in the crown of the precentral gyrus (Fig.1). Single biphasic TMS pulses were applied over multiple sites overlaying the

right precentral hand knob. TMS was performed with a cooled MC-B35 figure-of-eight coil connected to a MagPro X100 stimulation device (Magventure, Farum, Denmark). We chose a MC-B35 TMS coil, because this coil is small with an average winding diameter of 35 mm diameter to maximize the focality of TMS. Participants were seated in an adjustable armchair with the neck supported by a head-rest during TMS mapping. The position of the TMS coil relative to the participant's head was continuously tracked in real time with frameless stereotactic neuronavigation (Localite GmbH, Bonn, Germany). Any changes in the TMS position and orientation relative to the scalp were registered and updated online in a 3D space and displayed to the examiner on a screen. Prior to sulcus-aligned TMS mapping, we located the motor hotspot position of the left FDI muscle using the standard trial-and-error procedure with the handle of the coil angled at 45-degree relative to the midsagittal line (Groppa et al., 2012). We then determined the resting motor threshold (RMT) of the left FDI muscle, using the Maximum-Likelihood Strategy using Parameter Estimation by Sequential Testing (MLS-PEST) approach (Awiszus, 2003).

The TMS-evoked motor responses were recorded with surface electromyography from relaxed left first FDI and ADM using a belly-tendon montage (Ambu Neuroline 700, Columbia, USA). Trial-wise acquisition of MEPs was controlled by Signal software and EMG data were stored on a computer for later offline analysis (Cambridge Electronic Design, Cambridge, UK). Surface EMG signals were recorded at a sampling rate of 10 kHz and bandpass filtered (20 Hz – 3000 Hz) with an eight channel DC amplifier (1201 micro Mk-II unit, Digitimer, Cambridge Electronic Design, Cambridge, UK).

Sulcus-aligned TMS mapping of the motor hand knob

Standard grid-based TMS mapping of corticomotor representations keeps the coil orientation of the TMS coil identical across all grid sites (Teitti et al., 2008; Diekhoff et al., 2011; Vaalto et al., 2011, 2016; Sarfeld et al., 2012; Ahdab et al., 2014, 2016). This procedure induces electrical tissue currents in the motor hand knob that enter the precentral crown at different angles at the maximally stimulated part of the crown, when placing the coil at different points of the grid. This is problematic because the angle at which the electrical current "hits" the precentral gyrus has a strong impact on the TMS-induced electric field (Thielscher et al., 2011). In addition many of these mapping studies showed considerable inter-individual variation in the

hotspot location, with some participants having the hot-spot located even in the pre-frontal regions (Teitti et al., 2008; Vaalto et al., 2011; Ahdab et al., 2014, 2016).

These considerations prompted us to develop a sulcus aligned TMS mapping procedure which adjusts the orientation of the TMS coil at each mapping site to the local curvature of the precentral gyrus (Raffin et al., 2015; Dubbioso et al., 2017; Raffin and Siebner, 2018). The procedure exploits the fact that the motor hand representation in the precentral gyrus can be readily identified on structural MRIs by its characteristic knob-like shape (Yousry et al., 1997). The TMS coil is centred on one of seven equidistant target sites placed along the individual gyrus-sulcus border of the hand knob. The coil orientation is adjusted at each target site in a way that TMS always induces the strongest currents in a direction that is perpendicular to the local orientation of the precentral gyrus. This secures that TMS induces the highest electrical field strength in the crown of the precentral hand knob at all stimulation sites.

In this study, we extended our linear sulcus-aligned TMS mapping approach into a two-dimensional TMS mapping procedure to identify inter-individual differences in the rostro-caudal peak location of corticomotor excitability in the precentral gyrus. We added four parallel lines rostrally to the central sulcus over the precentral gyrus (Fig.1A). Each of the five parallel lines consisted of seven equidistant targets covering the entire longitudinal extension of the hand knob (35 target sites in total). The distance between two neighbouring target sites on the line was 5 mm. The first two lines covered the posterior lip of the precentral crown and the remaining three lines the top (apex) and anterior lip of the precentral gyral crown (Fig.1A). We reasoned that a sulcus-aligned mapping approach would be more sensitive than standard grid-based mapping with a conventional figure-8-coil to detect very small inter-individual variations of hotspot location. Indeed, personalization to the Pre-CS shape and a short inter-line distance rendered our approach more sensitive to subtle shifts in hotspot location in the Pre-CS.

TMS mapping was stereo-tactically guided using frameless neuronavigation (Localite GmbH, Bonn, Germany). First, the head of the subject was co-registered with the individual high-resolution anatomical MRI of the brain via anatomical landmarks (e.g., nasion and crus helicis) by using the surface mapping function of Localite. The root mean square differences between positions of landmarks in the MRI volume and at the subjects head were ≤ 2 mm for any TMS session of this study. Furthermore, to verify the quality of the co-registration procedure, we attached small vitamin E capsules (providing a good MRI T1 contrast) to a

volunteer's head at different anatomical positions. The software depicted and true positions of the capsules did not show mismatches larger than 1 mm for any position.

The brain surface, derived from the individual T1-weighted MRI, was rendered online and the sites to be targeted by TMS in the precentral gyrus were marked as dots on the segmented brain of each subject (Fig.1A). Based on anatomic landmarks, a trained investigator (R.D.) manually placed thirty-five stimulation sites: seven targets for five lines. As in our recent sulcus-aligned mapping studies (Raffin et al., 2015; Dubbioso et al., 2017; Raffin and Siebner, 2018), we chose a biphasic TMS pulse configuration. Biphasic pulse configurations are more efficient to stimulate the $M1_{HAND}$ than monophasic pulses (Lang et al., 2006). This allowed to use of a very focal coil without any heating problems, increasing focality compared to standard coils. The second phase of the biphasic stimulus always produced a current in the precentral gyrus with a caudal-to-rostral (posterior-anterior) direction perpendicularly to the local curvature of the central sulcus (Kammer et al., 2001).

To avoid carry-over effects between consecutive stimuli, inter-stimulus intervals were jittered between 4 and 5 s. For each target, we delivered 20 pulses in two 10-stimuli blocks at an intensity set to 120% of the conventionally defined RMT for left FDI muscle. At this stimulation intensity, we reliably evoked motor responses in the left FDI and ADM muscle. The order of stimulated precentral targets was pseudo-randomized across subjects with a fixed target sequence within a subject. The individual coil positioning parameters were stored by the neuronavigation software for each stimulation position (Localite GmbH, Bonn, Germany).

Data analysis

Motor evoked potentials

After the experiment, the EMG recordings were visually inspected to remove trials with significant artefacts. The peak-to-peak amplitude of each motor evoked potential (MEP) was extracted trial-by-trial using Signal software (Signal Version 4.02 for Windows, Cambridge Electronic Design, Cambridge, UK) in the time window between 10 and 40 ms after the TMS stimulus. For each of the 35 cortical targets, we determined mean peak-to-peak MEP amplitude and used the mean MEP amplitude to generate muscle excitability maps

for the ADM and FDI muscles along the precentral gyrus (Fig.1B). The resulting map indicated the site at which the mean MEP amplitude reached its peak. This "MEP peak" indicates the individual location of the motor hotspot in the precentral hand knob. Please note that we used the motor hotspot location derived from sulcus-shape based TMS mapping for all further analyses. The conventionally identified hotspot location that we had determined by trial-and-error at the start of the experiment to determine RMT was only considered in the analyses involving the simulation of the TMS-induced electrical field strength. In addition, we tested stability and reproducibility of this procedure on a single subject by replicating the TMS mapping procedure one week later. We used a custom-made software to extract the MNI normalized stereotactic x-, y- and z-coordinates, reflecting the cortical projection of the precentral motor hotspot as revealed by our sulcus-aligned mapping procedure.

We hypothesized that in individuals with a more rostral (anterior) precentral hotspot, TMS elicits premotor cortical excitation more up-stream to $M1_{HAND}$ than in individuals with a more posterior (caudal) precentral hotspot. We therefore expected that individuals with a rostral hotspot should also show longer MEP latencies than individuals with a caudal motor hotspot location in the precentral crown. Therefore, we determined the shortest MEP latency for the FDI and ADM muscle for each subject at the motor hotspot location. The shortest latencies were identified and measured by visual inspection of superimposed MEP waveforms (Chen et al., 2008; Groppa et al., 2012). This measurement was done by an experienced neurophysiologist (PJS) who was blinded with respect to the protocol set-up. We opted for corticomotor latency, because this measure had been employed in previous studies (Hamada et al., 2013; Volz et al., 2015) that successfully explore intra-individual effects of changing current direction on corticomotor conduction time, but acknowledge that the estimation of corticomotor conduction time would have been preferable to minimize the contribution of peripheral motor conduction time (Groppa et al., 2012).

Cortical thickness, folding and myelination

Cortical reconstruction was performed with the FreeSurfer image analysis suite ver. 6.0.0 (http://surfer.nmr.mgh.harvard. edu/) (Fischl and Dale, 2000). Using this approach, the grey and white matter surfaces were defined by an automated brain segmentation process. If required, an experienced investigator manually corrected the automated segmentation, following the procedures outlined at

https://surfer.nmr.mgh.harvard.edu/fswiki/Edits. The processes of surface extraction and inflation generated a number of well-known feature descriptors for the geometry of the cortical surface. These included: surface curvature estimated from the mean curvature (or average of the principal curvatures) of the white matter surface (Pienaar et al., 2008); cortical thickness estimated at each point across the cortex by calculating the distance between the grey/white matter boundary and the cortical surface. Individual whole brain surface maps were smoothed with a 5 mm 2D Gaussian smoothing kernel (Fischl and Dale, 2000) and the effect of surface curvature on cortical thickness was regressed out (Glasser et al., 2016). Using the FreeSurfer spherical registration method, the individual curvature-corrected cortical thickness maps were registered to a common FreeSurfer template surface (fsaverage) for visualization and group analysis (Fig.1D) (Fischl, 2012).

The data of the multiparameter mapping protocol was processed using a Voxel-Based Quantification (VBQ) toolbox developed for SPM8 (www.fil.ion.ucl.ac.uk/spm/).

Because curvature-associated modulations of myelination can obscure or distort myelination changes due to other variations in cyto- and myelo-architectonics (Annese et al., 2004), we have regressed out curvature and used for analysis the curvature-corrected R1-value variations, smoothed with a 5 mm 2D Gaussian smoothing kernel (Fischl and Dale, 2000). The individual maps were registered onto the FreeSurfer group template for visualization and group analysis (Fig.1C).

We were primarily interested in estimating regional cortical myelination as reflected by R1-values derived from quantitative structural MRI in the right precentral gyrus forming the motor hand knob. Therefore, we defined the right motor hand knob as precentral region-of-interest (ROI), covering the $M1_{HAND}$ and the adjacent PMd directly anterior to it. Within this ROI, we separately defined the Caudal Pre-Central Gyrus (Pre-CG), namely the gyral wall facing the central sulcus and the Rostral Pre-CG, the gyral crown and gyral wall facing Pre-central sulcus. The border between the Caudal and the Rostral Pre-CG was manually delineated on the average group image generated in freesurfer by using a line perpendicular to the cortical surface originating at the maximal convexity of the posterior lip region.

Then, the medio-lateral and antero-posterior borders of the overall ROI were defined based on the grid we used for precentral TMS mapping to achieve a reliable comparison of the MRI and TMS data. First, we considered the border of the grid by taking the grand mean of MNI normalized stereotactic x-, y- and z-

coordinates of the stimulation points forming the grid border of all participants. These coordinates were then projected on the flat FreeSurfer template surface (fsaverage) by using a custom-made matlab script. Each point was then connected to form a rectangle with a size of approximately 2 x 3 cm, using the function tksurfer_labeledit implemented in the Fresurfer software package. The rectangle was finally projected onto the pial surface (Fig. 2A). Individual mean cortical thickness values and R1-based cortical myelination estimates were extracted from the two precentral ROIs and used for correlational analyses.

Task-related fMRI and behavioural data

We used the Statistical Parametric Mapping (SPM) software package (SPM8; Wellcome Department of Imaging Neuroscience, London, UK, http://www.fil.ion.ucl.ac.uk) for pre-processing and statistical analysis of the functional MRI data. The first four volumes of a session (dummy images) were discarded from further analysis. Whole-brain EPIs, including reversed-phase EPI, were recorded to facilitate the accurate registration of the EPI data to the individual T1-weigthed image. The EPI time series was motion corrected, brain extracted and smoothed with a 1 mm two-dimensional Gaussian smoothing kernel (Fischl and Dale, 2000). We choose a small smoothing kernel to minimize the smearing of task-related somatosensory processing in the postcentral gyrus into the precentral gyrus.

We specified a first-level general linear model to assess differences in brain activity between the movement and rest blocks for each hand muscle. Two regressors-of-interest were defined for the blocks requiring isometric abduction movements of the left index finger (engaging the FDI muscle) or little finger (engaging the ADM muscle). To account for shifts in the onset of the hemodynamic response, temporal derivatives of the resulting time courses, motion, respiration and cardiac cycle were included in the model as regressors-of-no-interest (Friston et al., 1997; Smith et al., 2004). After model estimation, z-statistical images were calculated for the resulting maps of the parameter estimates and a corrected statistical threshold of $p<0.05$ was applied at the cluster level based on Gaussian random field theory (Worsley et al., 1996). The cluster extent threshold was set to an uncorrected $p < 0.001$ (here corresponding to a Z-score of 3.2). For reporting, the Z-statistical images were projected into Montreal Neurological Institute (MNI) space based on a nonlinear registration of the T1-weighted structural MRI on the MNI152 template (using FSL FNIRT; http://fsl.fmrib.ox.ac.uk/fsl/slwiki). In addition, average activation maps across subjects were rendered on the

FreeSurfer group template (figure 1) for visualization using the registration procedures as described in the online FreeSurfer tutorial (https://surfer.nmr.mgh.harvard.edu/fswiki/FsTutorial/FslFeatFreeSurfer).

During the visually cued isometric finger abduction task, we extracted the mean interval between two consecutive isometric contractions (i.e., inter-movement interval), its standard deviation (SD). Specifically, the signal was thresholded at a level of 0.6 V and the findpeaks matlab function was used to identify peaks with a minimum distance of 400 ms and a peak prominence of 1/3 of the maximum force value exerted by the subject. As the movement onsets were quite steep, we found it reasonable to use these peaks to define movement intervals. Importantly, the limited dynamic range of the force measurement setup caused the exerted force to often go beyond the maximum, this meant that the force measurements were only of limited practical use in this setting. Lastly, we calculated the coefficient of variation (CV) by dividing the SD with the mean to quantify between-trial dispersion of movement timing. The CV of the inter-movement interval indicates how well participants reproduced the one-per-second interval as signalled by the visual cue.

Electric field simulations

For each participant, we performed simulations of the electric fields that were generated in the right precentral gyrus by the TMS pulse using SimNIBS software 2.0 (www.simnibs.org). A realistic head model was automatically generated for each participant from the individual T1-weighted and T2-weighted MR images as described elsewhere (Thielscher et al., 2015). Electric field simulations were calculated for the coil position which elicited the highest mean MEP amplitude (i.e., the individual precentral motor hotspot) in left FDI muscle and a stimulation intensity scaled to the individual RMT of FDI to clearly visualize the effect of gyral anatomy on TMS-induced field strength. The TMS-related parameters to compute the E field strength (i.e., coil location, stimulus intensity) were obtained before the main TMS mapping experiment, when we conventionally determining the individual RMT of the FDI muscle by trial-and-error (Groppa et al., 2012). Hence, the E-field calculations represent the maps that one normally would derive in standard TMS experiments at the individual precentral motor hot spot. The vector potential of the MC-B35 coil was pre-calculated using a coil model consisting of a superposition of 1248 magnetic dipoles, as described in Thielscher and Kammer (Thielscher and Kammer, 2004). To obtain average electric fields across subjects, the electric fields were interpolated in the middle of the segmented cortical grey matter, and transformed to

the FSAverage template (Fischl, 2012) for second-level group analyses. We then created a group map of the electrical field distributions for the motor hotspot locations and statistically compared the TMS-induced electrical field distributions in the right precentral hand knob between the $M1_{HAND}$ and PMd group. Since the rostral $M1_{HAND}$ is confined to the posterior lip region of the precentral gyrus (Geyer et al., 1996), we hypothesized that the $M1_{HAND}$ group should display a higher electrical field magnitude in the posterior lip region relative to the PMd group.

Statistical group analyses

All the statistical computations were performed using IBM SPSS Statistics software (Version 22 for Windows, New York City, USA). Before applying parametric statistical tests, the normal distribution of all variables was verified by means of a Kolmogorov and Smirnov test.

In a first set of analyses, we explored the structural, functional and |E| field properties of the rostral and caudal part of the precentral motor hand knob. Individual estimates of myelination (derived from R1-mapping), cortical thickness (derived from T1-weighted MRI scans), mean electric field strengths, and mean task-related BOLD signal increase for index and little finger movements were extracted from the two precentral ROIs in the right precentral hand knob, corresponding to the caudal Pre-CG and rostral Pre-CG. For each variable, we computed separate paired t-tests to assess morpho-functional differences between the two precentral ROIs. Finger movement (index vs little finger) was included as additional within-subject factor in the ANOVA models analysing fMRI data and related performance measures.

A second set of analyses focused on the neurophysiological data recorded during sulcus-shape based TMS mapping of the left FDI and ADM muscle. Our primary interest was to capture inter-individual differences in cortico-muscular representation in the right precentral motor hand knob along the anterior-posterior axis. To quantify inter-individual variation in rostro-caudal cortico-muscular representation, we derived a composite measure for each participant that integrated the spatial (y-coordinate of precentral motor hot spot) and the temporal dimension (corticomotor MEP latency at motor hot spot) of hot-spot rostrality. We reasoned that the most robust way of quantifying functional rostrality of the corticomotor representation would be to derive a composite measure that integrates both, the spatial and temporal dimension of functional rostrality. The spatial dimension specifies how far the primary site of stimulation is away from the corticospinal output

neurons and the temporal dimension reflects how long does it take from the primary side to induce a transsynaptic excitation of the corticospinal output neurons.

In each participant, we first took the shortest MEP latency that had been obtained at the motor hotspot for both ADM and FDI muscles, and the corresponding y-coordinate of the respective muscle. We normalized each measure by scaling it between 0 and 1, with 0 corresponding to the shortest latency and the most posterior hotspot and 1 to the longest latency and most anterior hotspot. The two normalized variables were then multiplied yielding a muscle- and subject-specific "hotspot rostrality index". To test whether the spatial and temporal dimensions of the hotspot rostrality index are related, we calculated the Pearson's correlation coefficient between the individual y-coordinate of the hot spot and the shortest MEP latency at motor hotspot for the respective muscle.

The third set of analyses addressed the main question of this study and tested for function-structure relationships in the right precentral motor hand knob. We hypothesized that inter-individual variations in precentral myelin content would account for between-subject differences in precentral motor function (i.e., hot spot rostrality and task-related activation) and task performance (i.e., temporal synchronization of repetitive finger movement). Using the mean R1-signal of the entire Pre-CG ROI as index of cortical myelination, we calculated the Pearson's correlation coefficient between the mean precentral R1-value and individual functional read-outs such as the spatiotemporal rostrality index of the precentral motor hot spot, mean task-related activation and the stability of the between-movement interval during the visually cued movement synchronization task. Correlation analyses were conducted for each muscle (motor hotspot rostrality) or finger (task-related activation and performance during the cued movement synchronization task). Significance threshold was set at $p<0.05$ and the Bonferroni procedure was used to correct for multiple comparisons performed in each set of analyses. Data are given as mean (±SEM) if not otherwise specified.

We computed several follow-up analyses. We repeated the correlational analyses using only the mean MRI signal from the rostral and caudal Pre-CG ROI to see whether linear structure-function relationships were evenly expressed in the two ROIs. We also performed the same set of analyses using mean cortical thickness rather than the mean R1-signal to exclude that the results were driven by differences in thickness of the precentral hand knob. We also computed exploratory correlational analyses to assess the relationship

between spatiotemporal hotspot rostrality of the FDI and ADM hot spots and functional MRI-based and behavioural read-outs.

To visualize the spatial expression of significant correlations at the voxel level within the right precentral hand knob, we computed additional surface-based analyses within the precentral ROI on the FsAverage template by using Freesurfer software. These analyses were performed vertex-wise, followed by cluster-wise corrections for multiple comparisons based on the method suggested by Hagler and colleagues (Hagler et al., 2006) (cluster-determining threshold: $p<0.001$, cluster-wise correction $p<0.05$). Age at the time of MRI and sex were included in the model as nuisance variable. Finally, a separate surface between group analysis was used to compare the spatial distribution difference of E-field between the two groups of participants (posterior lip stimulation vs top of crown stimulation). Since we had a highly specific anatomical hypothesis (posterior lip region), the explorative between-group analysis of electrical field distribution in precentral gyrus applied a more liberal cluster extent threshold of $p<0.01$.

Results

Cortical myelination, thickness and curvature

The structural properties of the right precentral hand knob were assessed with quantitative structural MRI, using the mean R1-value of caudal and rostral part of the Pre-CG as index of regional myelination (see methods section for details). The R1-value was only available in 20 of the 24 subjects, as the quantitative MRI data of four subjects had to be excluded because of head movement related artefacts. The caudal part of the Pre-CG showed higher mean R1 values than its rostral part (Caudal Pre-CG ROI: 796.48 ± 8.51 ms^{-1} vs rostral Pre-CG ROI: 756.75 ± 9.29 ms^{-1}, paired t-test: $t_{(19)} = 5.069$, $p < 0.001$, Fig. 2B). We also ran voxel-wise analysis and surface rendering to visualize the regional expression of R1-values which showed that the regional R1 signal gradually decreased along a caudal-to-rostral gradient in the precentral hand knob (Fig.2B). To capture macrostructural features of the precentral motor hand knob, we derived cortical thickness and curvature from the T1-weighted MRI images. On average, the cortex was thicker in the rostral part of the precentral motor hand knob than in its caudal part (Caudal Pre-CG ROI: 2.51 ± 0.04 mm vs rostral Pre-CG ROI: 2.73 ± 0.03 mm, paired t-test: $t_{(23)} = -6.431$, $p < 0.001$, Fig. 2D). Cortical folding, indexed by regional mean curvature was larger in the caudal part than in the rostral part of the precentral

motor hand knob (Caudal Pre-CG ROI: 0.02 ± 0.01 mm^{-1} vs rostral Pre-CG ROI: -0.08 ± 0.01 mm^{-1}, paired t-test: $t_{(23)} = 42.368$, $p < 0.001$).

Precentral corticomotor representations

In each participant, the mean peak-to-peak MEP amplitude at each cortical stimulation site was used to create two-dimensional maps of the corticomotor representations of the FDI and ADM muscle (Fig. 3A). This enabled us to identify the precentral motor hotspot for each muscle, i.e. the stimulation site at which mean MEP amplitude was largest. Mean MEP amplitude at motor hotspot was 1.11 (± 0.17) mV for the FDI muscle and 0.50 (± 0.08) mV for the ADM muscle, reflecting the fact that MEP amplitudes were overall larger for the FDI muscle. Since we mapped the spatial representation of MEP amplitudes along five parallel lines in parallel to the curvature of the precentral gyrus, we were able to estimate the "rostrality" of the individual hotspot along the anterior-posterior dimension of the precentral gyrus. In agreement with our hypothesis, the position of individual motor hotpots along the rostro-caudal direction varied across participants. Based on the rostrality of precentral hotspot location, we assigned participants to a "rostral hotspot" group in which the hotspot located on one of the three anterior lines (n= 14) or to a "caudal hotspot" group in which the hotspot located on one of the two posterior lines close to the central sulcus (n= 10). Table 1 summarizes mean group data for the entire group as well as for the rostral and caudal hotspot sub-group separately. Groups were matched in terms of overall efficacy to excite the corticomotor output (table 1). Mean MEP amplitudes at hotspot and cortical excitation thresholds for evoking a motor response did not differ between the rostral and caudal hotspot sub-group for both muscles (FDI muscle: t(22)= 14.461, p= 0.434; ADM muscle: t(22)= 21.611, p= 0.503; unpaired t-test).

We extracted the stereotactic coordinates to systematically assess the topographical distribution of the motor hotspots in the precentral motor hand knob. Using the stereotactic hotspot coordinates as dependent variable, we computed a mixed-model ANOVA using group assignment as between-subject factor and *hand muscle* (FDI vs ADM muscle) and *axis of stereotactic coordinate* (x-, y-, and z-direction) as within-subject factors. The ANOVA validated our group assignment, showing an interaction between *coordinates* and *group* ($F_{(2,44)}= 6.049$, $p=0.005$). Post-hoc analyses were performed to test for between-group differences of hotspot locations along the x-, y-, and z-directions. The "rostral hotspot" and "caudal hotspot" groups only differed

with respect to their y-coordinates, corresponding to the sagittal (anterior-posterior) dimension in stereotactic space. Mean y-coordinates of both muscles was -21.5 ± 1.3 in the "rostral hotspot" group and -14.1±0.7 in the "caudal hotspot" group ($t(22)= -7.382$; $p<0.001$; Bonferroni-corrected t-test). The ANOVA also showed an interaction between *coordinates* and *muscle* ($F_{(2,44)}= 8.299$, $p=0.001$), confirming a significant difference in precentral location between the FDI and ADM motor hotspots. Specifically, ADM muscle was located more medially ($t(22)= 3.312$; $p=0.005$; Bonferroni-corrected t-test) and superiorly ($t(22)= -2.598$; $p=0.005$; Bonferroni-corrected t-test) relative to the hotspot of the FDI muscle. This finding replicates our previous sulcus-aligned mapping studies, using a single line of targets placed at the caudal border of the precentral crown (Raffin et al., 2015; Dubbioso et al., 2017; Raffin and Siebner, 2018). Finally, ANOVA also revealed main effects of the factors *group* ($F_{(1,22)}= 47.491$, $p<0.001$) and *coordinates* ($F_{(2,44)}= 251.644$, $p< 0.001$).

Spatiotemporal "rostrality" of precentral motor hotspot

We hypothesized that the "spatial rostrality" of the motor hotspot scaled linearly with its "temporal rostrality" resulting in longer cortico-to-motor conduction time. We therefore tested for a positive linear relation between the antero-posterior coordinate (y) of the motor hotspot and the shortest MEP latency evoked at the hotspot. We found that individual corticomotor latencies scaled positively with spatial rostrality of individual motor hotspot locations in the precentral hand knob (Fig.3B). The more anterior (rostral) the motor hotspot was located along the anterior-posterior (sagittal) direction, the longer was corticomotor latency. Considering the data of all participants, we found a significant positive linear relationship between y-coordinate of the motor hotspot and shortest MEP latency at hotspot, both for the FDI muscle ($r= 0.697$, $p< 0.001$) and ADM muscle ($r= 0.555$, $p= 0.005$). No such relationship was found for the medio-lateral x-coordinate (Fig.3B) and superior-inferior z-coordinate (FDI muscle: $r= 0.084$, $p= 0.697$; ADM muscle: $r= 0.109$, $p=0.614$). This association confirms our hypothesis that cortical precentral excitation occurs functionally more "up-stream" to the cortico-motoneuronal neurons, when the preferential target site is located more rostrally in the crown of the precentral hand knob.

Our sulcus-aligned TMS mapping procedure yielded a spatial (y-coordinate) and a temporal (MEP-latency) rostrality measure of the individual TMS target site in the gyral crown of the precentral hand knob. Considering both, the spatial and temporal rostrality dimensions, we computed a "spatiotemporal rostrality

index" of the TMS hotspot (see Methods section for details). This spatiotemporal rostrality index reflects how much TMS preferentially excites cortical neurons in the caudal PMd or $M1_{HAND}$. At the individual level, the spatiotemporal rostrality index of the FDI and ADM muscle showed a positive linear relationship ($r= 0.819$, $p<0.001$), showing that hotspot rostrality of the two hand muscles was consistently expressed at the single-subject level.

Precentral myelination scales with spatiotemporal rostrality of precentral motor hotspot

The regional myelination of the precentral hand knob as indexed by the mean R1-value showed a significant positive linear relationship with individual spatiotemporal rostrality index. The higher the mean R1-signal in the right precentral hand knob, the higher was the rostrality index of the precentral motor hot spot (Fig.4). This positive relationship was found for the FDI hotspot ($r= 0.699$, $p<0.001$, Fig.4A) and ADM hotspot ($r= 0.637$, $p= 0.003$, Fig.4C). Surface-based correlation analyses pinpointed a rostro-lateral cluster in the anterior lip region of the precentral crown where regional R1-values correlated most strongly with the individual spatiotemporal rostrality index with peak correlation at x, y, z = 32.6, -11.3, 53.6 for the FDI muscle (Fig.4B) and at x, y, z = 34.8, -11.6, 59.2 for ADM muscle (Fig.4D). A second cluster was located dorsal and medially in the posterior lip region of the precentral gyrus. Correlation peaked at x, y, z = 26.6, -22.7, 51.8 for the FDI muscle and at x, y, z = 29.3, -21.8, 58.7 for the ADM muscle. Both hand muscles expressed a positive linear relationship in the caudal Pre-CG (FDI muscle: $r= 0.720$, $p< 0.001$; ADM muscle: $r= 0.591$, $p= 0.006$) and rostral Pre-CG (FDI muscle: $r= 0.625$, $p= 0.003$; ADM muscle: $r= 0.571$, $p= 0.007$).

At the individual level, regional thickness of the right precentral gyrus did not predict spatiotemporal rostrality of the precentral motor hotspot. No significant correlation was found between cortical thickness and the individual rostrality index for both muscles (FDI muscle: $r= -0.230$, $p= 0.280$; ADM muscle: $r= -0.277$, $p= 0.190$). There was also no significant correlation between mean curvature of the right precentral gyrus and the rostrality index for both muscles (FDI muscle: $r= 0.146$, $p= 0.495$; ADM muscle: $r= -0.021$, $p= 0.924$). Together, these negative results show that the association between regional myelination and spatiotemporal rostrality of the precentral hotspot was not driven by differences in cortical volume and mean curvature.

Myelination of the precentral hand knob has functional and behavioural correlates

Our multimodal mapping approach revealed a link between cortical myelin content and functional cortico-motor representations in the precentral motor hand knob and timing proficiency during stereotyped finger movements. While the right precentral motor hand knob was consistently activated when participants performed visually cued finger movements at a repetition rate of 1Hz, the rostral part of the precentral Mean task-related BOLD increase was stronger in the caudal Pre-CG ROI (1.6 ± 0.13) compared to the rostral Pre-CG ROI (1.26 ± 0.09), paired t-test: $t_{(23)} = 3.401$, $p = 0.002$ (Fig.2C). We tested whether the degree of precentral myelination predicts the magnitude of task-related regional activation and task performance. We found a positive linear correlation between the mean cortical R1 signal within the precentral motor hand knob and the magnitude of cortical activation during the visuo-motor synchronization task (Fig.5). This positive relationship was found regardless of whether the task was carried out with the index ($r= 0.659$, $p= 0.002$, Fig.5A) or little finger ($r= 0.748$, $p<0.001$, Fig.5C). Surface-based correlation analyses located the regional expression of this relationship to a rostro-lateral cluster in the anterior lip region of the precentral crown where regional R1-values correlated most strongly with regional task-related activation during repetitive movements with the index finger (peak correlation at x, y, z = 28.3, -14.4, 63.1; Fig.5B) or little finger (x, y, z = 27.6, -14.1, 65.2; Fig.5D). The linear relationship between cortical myelination and task-related activation was expressed in the rostral precentral ROI (FDI muscle: $r= 0.655$, $p= 0.002$; ADM muscle: $r= 0.554$, $p= 0.011$), but also in the caudal precentral ROI for the ADM muscle ($r= 0.591$, $p= 0.006$) and trend-wise for the FDI muscle ($r= 0.404$, $p= 0.078$).

Precentral myelination did not only predict task-related BOLD signal changes in the precentral motor hand knob, but also the temporal reliability of movement repetition in the visuomotor synchronization task (Fig.6) We found that participant more precisely synchronized their finger movements to the external pace, the higher the precentral myelin content. There was a significant negative linear relation between precentral cortical myelination, as indexed by regional R1-value, and the mean CV of movement repetition rate for both fingers, index finger: $r= -0.619$, $p= 0.004$ and little finger: $r= -0.684$, $p< 0.001$ (Fig. 6A, C). This indicates that individuals with a higher degree of cortical myelination of the precentral gyrus showed a more regular timing of repetitive finger movements with less inter-trial variation of the between-movement interval. Surface-rendered maps of this relationship at voxel levels yielded several clusters which were mainly

located, but not limited, in the precentral crown (Fig.6B, D). Follow-up analyses based on the mean R1-signal from the two Pre-CG ROIs revealed that the myelin content in the rostral (index finger: r= -0.601, p= 0.004; little finger: r= -0.662, p= 0.001) and caudal part of the motor hand knob (index finger: r= -0.590, p= 0.006; little finger: r= -0.626, p= 0.003) scaled negatively with the mean CV of movement repetition rate for both fingers.

We also performed exploratory analyses in which we tested for linear relationships between hotspot rostrality and functional motor read-outs (FDI muscle: r= 0.450, p= 0.031; ADM muscle: r= 0.525, p= 0.008). Like for the mean R1-signal in precentral gyrus, we found that inter-individual variations in BOLD-signal change and movement repetition rate also scaled linearly with individual hotspot rostrality, showing that this functional TMS readout also reflects inter-individual differences in cortical motor function at the level of regional neural activity and timing performance (FDI muscle: r= -0.617, p= 0.0013; ADM muscle: r= -0.619, p= 0.0013).

Hotspot location is related to induced electrical field magnitude in precentral gyrus

Since all participants underwent structural T1-weighted and T2-weighted MRI scans, we were able to simulate the electric fields that were generated in the right precentral gyrus by the TMS pulse at the individual precentral hotspot as determined in the preparatory TMS session. We first created a group map of the electrical field distributions for the motor hotspot locations. Electric field strength was high in the precentral crown and weak in the sulcal parts of the precentral gyrus (Fig. 2E). We statistically compared the TMS-induced electrical field distributions in the right precentral hand knob between the group with a rostral or a caudal hotspot location in the main experiment (Fig. 7). The colour-coded surface rendered maps of the regionally induced electrical field confirmed that the average of electric field strength was maximal in the precentral crown corresponding to the precentral hand knob with additional local peaks with lower intensity in neighbouring gyral crowns (Fig.7A,B). Although the spatial distribution of the TMS-induced electrical fields was similar in the right precentral hand knob, between-group comparison revealed higher electrical field magnitudes in the posterior lip region in the group having a more caudal hotspot location in the shape-based TMS mapping experiment (Fig.7). The between-group difference in electrical field magnitude peaked at the x-,y-,z-coordinates 34, -20, 65, corresponding to the posterior lip region of the precentral gyrus. The

group with a more rostral motor hotspot did not display any clusters in the precentral gyrus where the induced electrical field was higher than in subjects with a more caudal hotspot location. Hence, electrical field strength did not differ between groups in the anterior lip region of the precentral gyrus. In a follow-up analysis, we tested whether the individual E-field strength in precentral gyrus scales would scale with precentral cortical myelin content. We found no cluster in the precentral gyrus showing a significant linear relationship between individual E-field strength and cortical myelin content.

Discussion

In healthy human volunteers, we probed the regional structure and function of the right precentral motor hand knob with TMS, structural and functional MRI. Our multimodal brain mapping approach revealed a link between cortical myelin content, functional cortico-motor representations, and dexterous motor control. A higher myelin content of the precentral motor hand knob was associated with more rostral corticomotor presentations as revealed by shape-informed TMS mapping, with stronger task-related activation during task-based fMRI, and a higher precision of movement timing during a visuo-motor synchronization task.

Relationship between precentral myelin content and rostrality of corticomotor muscle presentations

The spatial location of the motor hotspot, defined as the optimal scalp position where TMS evokes a contralateral motor response, varied across individuals along an anterior-posterior axis. In contrast to standard grid-based mapping, our sulcus-aligned mapping procedure secured that TMS at each stimulation site produced a consistent current direction in the most strongly stimulated part of the precentral hand knob regardless of the individual folding pattern. Extending previous work, we found that a more rostral hotspot location in the precentral crown was associated with a longer corticomotor MEP latency. In individuals, in whom the motor hot spot was spatially more distant from the central sulcus, stimulation also occurred functionally more upstream from the corticospinal motoneurons, resulting in longer latencies. In other words, “spatial” rostrality of the individual motor hotspot was mirrored by a “temporal” or “functional” rostrality of the motor hotspot. MRI mapping of the R1 signal revealed that the spatiotemporal “hotspot rostrality” had a structural correlate in the precentral hand knob. The degree of precentral myelination, reflected by the mean regional R1 signal, but not cortical thickness scaled with inter-individual differences in spatiotemporal “hotspot rostrality”.

675

676 ***TMS of the motor hand knob is spatially biased towards the superficial crown-lip region***

677 The human M1-HAND consists of a posterior (or caudal) region which is located in the depth of the anterior
678 sulcal wall (referred to as BA4p) and an anterior (or rostral) region (referred to as BA4a) which is located
679 more superficially in the anterior wall and may expand into the superficial crown-lip region (Geyer et al.,
680 1996,2000). Retrograde tracing studies in the macaque monkey identified the caudal portion of M1 in the
681 anterior bank of the central sulcus as the main precentral source of cortico-motoneuronal pyramidal output
682 neurons (Rathelot and Strick, 2006, 2009). The number of fast-conducting corticospinal pyramidal output
683 neurons with direct synaptic connections to the cervical motoneurons are mainly found in the caudal "new"
684 portion of the M1-HAND corresponding to area BA4p in humans (Rathelot and Strick, 2006, 2009). Since
685 the vast majority of fast-conducting corticospinal pyramidal output neurons originate from the caudal M1-
686 HAND in the depth of the central sulcus, these neurons but also the axons of other interneurons and
687 pyramidal cells in caudal M1-HAND (BA4p) are "out of reach" for the TMS-induced electrical field which
688 primarily targets the superficial crown-lip region in the precentral gyrus. We therefore argue that cortical
689 regions that are located more superficially and are functionally more "upstream" such as the rostral M1-
690 HAND (BA4a) and the caudal part of PMd are the primarily excited cortical areas, when TMS is applied to
691 the motor hot spot. The primary stimulation of superficial precentral areas then causes a transsynaptic
692 (indirect) excitation of fast-conducting corticospinal output neurons via cortico-cortical axonal projections
693 from anterior M1-HAND and the caudal part of PMd to the posterior M1-HAND (Siebner, 2020).
694 A recent biophysical modelling study identified axonal terminations in the crown-lip region of the precentral
695 gyrus, that are aligned to the locally induced e-field direction, as primary target structures for TMS-induced
696 neuronal excitation (Aberra et al., 2020). Efficient excitation of axonal terminations within the precentral
697 crown-lip region will lead to transsynaptic excitation of other cortical neurons in this area (i.e., axonal-
698 termination hypothesis). The highly synchronized neuronal activity in the stimulated crown-lip region may
699 then spread to deeper parts of the precentral cortex (especially the caudal M1-HAND) in the sulcal wall via
700 cortico-cortical axonal fibers. Alternatively, it is possible that the induced electrical field primarily stimulates
701 the bends of juxtacortical cortico-cortical axons that originate in the precentral crown and project into the
702 depth of the sulcus where the bulk of the fast-conducting corticospinal motoneurons are located (i.e., axonal-

bend hypothesis). Electric field modelling suggests that the field strength in juxta-cortical white matter of the precentral crown is indeed higher than the field strength in the overlying gray matter (Thielscher et al., 2011), and axonal bends have been identified as putative stimulation sites based on morphologically simplified neural models (Salvador et al., 2011).

Direction-specific target engagement of axonal structures in the precentral crown

We used biphasic TMS pulses for shaped-informed TMS mapping as in our previous studies (Raffin et al., 2015; Dubbioso et al., 2017; Raffin and Siebner, 2018). The biphasic pulse produced two neurobiologically relevant currents in the precentral gyrus: the first phase of the biphasic pulse produced an Anterior-to-Posterior (A-P) directed current, while the second phase caused a current with a Posterior-to-Anterior (P-A) direction. The second P-A component is neurobiologically most effective given the longer duration and larger area-under-the-curve, but the first A-P component may also induce action potentials and contribute to the MEP. The direction-dependent effects of the A-P and P-A components of the biphasic pulse may determine the anterior-posterior hot spot location. In their modelling study, Aberra et al. (2020) showed that a monophasic TMS pulse producing an A-P directed current in the precentral gyrus resulted in an anterior shift of activation of axon terminals of pyramidal neurons in layer two or five compared to a monophasic TMS pulse causing a current in the opposite (P-A) direction. Interestingly, this pattern also emerged albeit to a lesser extent, when simulating the precentral crown with a biphasic pulse configuration (Aberra et al., 2020). This implies that a P-A directed current will result in lower thresholds for efficient axonal depolarization in the posterior lip region, while an A-P directed current will result in lower excitation thresholds in the anterior lip region of the crown. The biophysical properties of biphasic TMS may account for the present results. The A-P component of the TMS pulse may have been more relevant for overall stimulation of axonal structures in the precentral crown in individuals with a more anterior precentral motor hotspot location: In these individuals, the A-P current may have been more effective to induce suprathreshold depolarization of axonal terminations in the anterior lip region. Conversely, the depolarizing effects of the P-A current may be more prevalent in individuals with a more posterior motor hotspot location. In these individuals, a preponderant excitation of axonal terminations in the posterior lip region may have shifted the precentral motor hotspot posteriorly. This explanation is corroborated by the simulations of the TMS-induced electrical field at the hot spot location. Here, TMS induced a stronger electrical field in the

posterior lip of the precentral crown only in individuals in whom sulcus-shaped TMS mapping revealed a caudal posterior precentral motor hotspot.

In addition to intracortical excitation of axon terminals, a biphasic TMS pulse may effectively depolarize longer-range juxtacortical axons at their bends in the subcortical white matter within the precentral crown-lip region. Since the depolarizing effect of the electrical field on the axonal bend depends on its orientation relative to the e-field, the A-P and P-A directed currents may result in spatially distinct hotspots. The A-P directed current preferentially stimulates axonal bends in more anterior (rostral) locations within the precentral crown, whereas the P-A directed current may preferentially stimulate axonal bends in more posterior (caudal) locations in the precentral crown. The capability to excite these axon bends may differ across individuals and thus, contribute to inter-individual variations in motor hotspot location.

Positive linear relationship between spatial and temporal hot spot rostrality

In our study, participants with a more rostral hotspot had longer corticomotor latencies than those with a more caudal hot spot location. The inter-individual variation in corticomotor latencies may be caused by the inter-individual variation in preferential A-P stimulation in the precentral crown. According to the axonal-termination hypothesis, a preferential stimulation of axonal terminations in the anterior lip region (A-P current) or posterior lip region (P-A current) of the precentral crown will alter the cortico-cortical conduction time from the precentral crown to the caudal M1-HAND (BA4p area) in the depth of the central sulcus. This explanation is in good agreement with previous TMS studies on the impact of a current reversal for monophasic pulse configurations: Reversing the current flow from PA to AP in the precentral crown also results in longer corticomotor latencies and higher corticomotor thresholds (Hamada et al., 2013) and stronger susceptibility to variations in pulse length (D'Ostilio et al., 2016). Furthermore, MEP-latency after AP-TMS was found to correlate with functional connectivity between M1 and a network involving cortical premotor areas (Volz et al., 2015).

The axonal-bend hypothesis may also explain the observed variation in corticomotor latency. The folding of the cortex at the gyral crown alters the curvature of axonal bends in the juxta-cortical part of the anterior and posterior lip region which renders these spatially segregated segments of the same axons more or less susceptible to the anterior-posterior phase of the biphasic TMS pulse. Accordingly, the A-P and P-A current

components of the biphasic pulse may stimulate the same juxta-cortical cortico-cortical axons at more anterior or posterior positions in the precentral crown. In humans, TMS activates neural elements having time constants determined from strength–duration curves of roughly 200 µs (Barker et al., 1991; Peterchev et al., 2013; D'Ostilio et al., 2016) with conduction times comparable to peripheral motor axons. A very conservative estimate would be that these axons have conduction speed of around 10 m/s (West and Wolstencroft, 1983; Firmin et al., 2014). In this case, the observed MEP latency differences would correspond to a travelled distance of >12 mm which is in the range of the observed variations of the hotspot in caudal-rostral direction. For a slightly less conservative estimate of conduction speeds of 20 m/s or more, the observed MEP latency differences are too long to be explained merely by the stimulation of two positions of the same axons anymore, but rather favours the targeting of different neural populations. Finally, the axon diameter distribution of cortico-cortical projection fibers within the precentral gyrus may have contributed to the between-subject variations in corticomotor latency (Liewald et al., 2014). The larger the cortico-cortical axons and the thicker their myelin sheets, the faster the signal transmission from the primary site of stimulation in the precentral crown to the fast-conducting corticospinal output neurons originating from the caudal M1-HAND (BA4p area) in the depth of the central sulcus.

Positive linear relationship between hotspot rostrality and precentral myelination

Our results establish a link between the myelination of the precentral hand knob and motor hot spot location, showing that the cortical myelin content scaled with individual motor hotspot rostrality. The axonal-termination hypothesis of TMS-induced cortex stimulation can account for this positive relationship. Stronger myelination of axons may lower the excitation threshold of axonal terminals in the anterior and posterior crown-lip region of the precentral gyrus to fire action potentials in response to TMS. This may be particularly relevant for the efficacy of the A-P component of the biphasic pulse which is less efficient than the P-A component. If axon terminations are more myelinated in the anterior lip region of the central gyrus, they will become more susceptible to the depolarizing effect of the A-P directed current. The A-P directed current will contribute more to the overall stimulation of axonal terminations in the precentral crown and shift the motor hotspot location to a more anterior location. Conversely, the motor hotspot will be located more caudally if the P-A component makes the strongest contribution to overall axonal depolarization in the precentral crown.

The axonal-bend hypothesis of TMS-induced cortex stimulation can also account for the positive relationship between hotspot rostrality and the degree of precentral myelination. If juxtacortical axonal bends in the anterior lip region are more strongly myelinated, they may be more easily depolarized by the A-P directed current. A relatively stronger contribution of the A-P directed current to the overall excitation of axonal bends in the precentral crown will result in an anterior shift of the motor hotspot.

A macro-anatomical perspective on spatiotemporal hotspot variability

Do the inter-individual differences in spatiotemporal hotspot rostrality indicate that TMS preferentially excites cytoarchitectoncially different cortex regions? The rostral M1-HAND (BA4a) and caudal PMd in the precentral crown-lip regions are the primary target regions, when TMS is applied at the precentral motor hot spot (Aberra et al., 2020). The border between rostral M1-HAND and caudal PMd is not sharply demarcated but smooth and the transition may vary considerable along the anterior-posterior axis in the precentral gyrus (Geyer et al. 1996, 2000). In some individuals, the transition zone between M1-HAND and PMd extends to the precentral crown-lip region, making the superficial part of the rostral M1-HAND a primary target for TMS, in individuals with a caudal motor hot spot location. Therefore, one should be cautious to conclude that in individuals with an anterior or posterior precentral hot spot, TMS preferentially stimulates more rostral or caudal parts of PMd, respectively. It is also possible that TMS preferentially stimulates the most anterior part of the rostral M1-HAND in individuals with a posterior precentral motor hotspot.

In macaque monkeys, intracortical electrical stimulation revealed that both, the rostral (old) and caudal (new) part of M1 send slowly conducting mono-synaptic corticospinal projections to the cervical motoneurons, while only the caudal (new) M1 hosted pyramidal cells with fast monosynaptic corticospinal projections to the cervical spinal motoneurons (Witham et al., 2016). In persons with a posterior precentral hotspot, the slowly conducting mono-synaptic corticospinal projections to the cervical motoneurons may be readily stimulated by TMS via excitation of local axonal terminals, if the rostral M1-HAND extends rostrally into the posterior crown-lip region.

Linking precentral myelination and motor function

Regional myelination showed a positive linear relationship with motor activation in the precentral hand knob during task-based MRI in the anterior lip region of the precentral crown. The stronger task-related engagement of the right caudal PMd in individuals with a higher precentral myelin content is in good agreement with previous work showing that the PMd plays a prominent role in visuomotor integration (Jäncke et al., 2000; Sugiura et al., 2001; Cerasa et al., 2005; Chouinard and Paus, 2006; Witt et al., 2008; Hardwick et al., 2015). We also identified several clusters in the rostral and caudal part of the precentral motor hand knob where a higher cortical myelin content was associated with a higher degree of temporal regularity during the finger tapping task. Our motor task probed temporal aspects of dexterous motor control, because participants had to match the timing of tapping to the regular one-hertz pace given by an external cue. Individuals with a higher precentral myelin signal were better at minimizing inter-trial variations between consecutive movements. We therefore argue that a higher degree of myelination of the precentral gyrus enabled a more precise synchronization of finger tapping with the regular pace provided by the visual cue.

How does cortical myelination support the integration of neuronal activity within functional brain networks? Structural MRI studies have linked cortical myelination to intrinsic functional connectivity (Huntenburg et al., 2017) and task-related functional activity in unimodal cortical areas, including the visual (Sánchez-Panchuelo et al., 2012; Sereno et al., 2013), auditory (Dick et al., 2012; Kim and Knösche, 2016), and sensorimotor cortex (Glasser et al., 2016; Kuehn et al., 2017). Axonal myelination enables fast signal propagation and synchronizes neural activity and determine properties of neuronal activity subserving temporal coding, such as spike latency and inter-spike interval (Seidl et al., 2010; Pajevic et al., 2014; Ford et al., 2015; Timmler and Simons, 2019). Our results lend further support to the notion that a high degree of myelination in adult neocortex is critical to fast and temporally precise, regional neuronal processing, suggesting that a high degree of precentral myelin content enables higher temporal precision during dexterous hand use.

Conclusion

We provide first-time evidence for behaviourally relevant, structural and functional phenotypic variation in the crown of the human precentral motor hand knob. Linking variations in regional brain structure and

function, regional excitability and dexterity, our results corroborate the functional relevance of cortical myelin for cortical function and related behaviour.

Our results are also of relevance to the research community that uses TMS of the human $M1_{HAND}$ to study motor cortex plasticity. Defining the individual precentral motor hotspot location is the standard method for spatial targeting of human $M1_{HAND}$ (Groppa et al., 2012; Rossini et al., 2015). Our work questions the assumption that hotspot-based targeting can secure a comparable stimulation of the precentral motor hand knob across subjects. In recent years, it has been emphasized that the plasticity-induced effects of repetitive TMS targeting $M1_{HAND}$ suffers from substantial inter-individual variability (López-Alonso et al., 2014; Ziemann and Siebner, 2015). Inter-individual differences in motor hotspot rostrality may constitute a major contributing factor to inter-individual differences in the after-effects on corticomotor excitability. Since inter-individual differences in hotspot rostrality are associated with different microstructural properties in terms of cortical myelination, it is possible that individuals with a more rostral or caudal motor hotspot may express different forms of precentral motor plasticity.

References

Aberra AS, Wang B, Grill WM, Peterchev A V. (2020) Simulation of transcranial magnetic stimulation in head model with morphologically-realistic cortical neurons. Brain Stimul 13:175–189.

Ahdab R, Ayache SS, Brugières P, Farhat WH, Lefaucheur JP (2016) The Hand Motor Hotspot is not Always Located in the Hand Knob: A Neuronavigated Transcranial Magnetic Stimulation Study. Brain Topogr 29:590–597.

Ahdab R, Ayache SS, Farhat WH, Mylius V, Schmidt S, Brugières P, Lefaucheur JP (2014) Reappraisal of

the anatomical landmarks of motor and premotor cortical regions for image-guided brain navigation in TMS practice. Hum Brain Mapp 35:2435–2447.

Annese J, Pitiot A, Dinov ID, Toga AW (2004) A myelo-architectonic method for the structural classification of cortical areas. Neuroimage 21:15–26.

Awiszus F (2003) Chapter 2 TMS and threshold hunting. Elsevier B.V.

Barker AT, Garnham CW, Freeston IL (1991) Magnetic nerve stimulation: the effect of waveform on efficiency, determination of neural membrane time constants and the measurement of stimulator output. Electroencephalogr Clin Neurophysiol Suppl 43:227–237.

Barker AT, Jalinous R, Freeston IL (1985) Non-invasive magnetic stimulation of human motor cortex. Lancet 1:1106–1107.

Bungert A, Antunes A, Espenhahn S, Thielscher A (2017) Where does TMS Stimulate the Motor Cortex? Combining Electrophysiological Measurements and Realistic Field Estimates to Reveal the Affected Cortex Position. Cereb Cortex 27:5083–5094.

Cerasa A, Hagberg GE, Bianciardi M, Sabatini U (2005) Visually cued motor synchronization: Modulation of fMRI activation patterns by baseline condition. Neurosci Lett 373:32–37.

Chen R, Cros D, Curra A, Di Lazzaro V, Lefaucheur JP, Magistris MR, Mills K, Rösler KM, Triggs WJ, Ugawa Y, Ziemann U (2008) The clinical diagnostic utility of transcranial magnetic stimulation: Report of an IFCN committee. Clin Neurophysiol 119:504–532.

Chouinard PA, Paus T (2006) The Primary Motor and Premotor Areas of the Human Cerebral Cortex. Neurosci 12:143–152.

D'Ostilio K, Goetz SM, Hannah R, Ciocca M, Chieffo R, Chen JCA, Peterchev A V., Rothwell JC (2016) Effect of coil orientation on strength-duration time constant and I-wave activation with controllable pulse parameter transcranial magnetic stimulation. Clin Neurophysiol 127:675–683.

Dick F, Tierney AT, Lutti A, Josephs O, Sereno MI, Weiskopf N (2012) In vivo functional and myeloarchitectonic mapping of human primary auditory areas. J Neurosci 32:16095–16105.

Diekhoff S, Uludağ K, Sparing R, Tittgemeyer M, Cavuşoğlu M, Von Cramon DY, Grefkes C (2011) Functional localization in the human brain: Gradient-echo, spin-echo, and arterial spin-labeling fMRI compared with neuronavigated TMS. Hum Brain Mapp 32:341–357.

898 Dubbioso R, Raffin E, Karabanov A, Thielscher A, Siebner HR (2017) Centre-surround organization of fast
899 sensorimotor integration in human motor hand area. Neuroimage 158:37–47.
900 Dum RP, Strick PL (2005) Frontal Lobe Inputs to the Digit Representations of the Motor Areas on the
901 Lateral Surface of the Hemisphere. J Neurosci 25:1375–1386.
902 Elston GN, Rockland KS (2002) The pyramidal cell of the sensorimotor cortex of the macaque monkey:
903 Phenotypic variation. Cereb Cortex 12:1071–1078.
904 Firmin L, Field P, Maier MA, Kraskov A, Kirkwood PA, Nakajima K, Lemon RN, Glickstein M (2014)
905 Axon diameters and conduction velocities in the macaque pyramidal tract. J Neurophysiol 112:1229–
906 1240.
907 Fischl B (2012) FreeSurfer. Neuroimage 62:774–781.
908 Fischl B, Dale AM (2000) Measuring the thickness of the human cerebral cortex from magnetic resonance
909 images. Proc Natl Acad Sci 97:11050–11055.
910 Ford MC, Alexandrova O, Cossell L, Stange-Marten A, Sinclair J, Kopp-Scheinpflug C, Pecka M, Attwell
911 D, Grothe B (2015) Tuning of Ranvier node and internode properties in myelinated axons to adjust
912 action potential timing. Nat Commun 6:8073.
913 Friston KJ, Buechel C, Fink GR, Morris J, Rolls E, Dolan RJ (1997) Psychophysiological and modulatory
914 interactions in neuroimaging. Neuroimage 6:218–229.
915 Geyer S, Ledberg A, Schleicher A, Kinomura S, Schormann T, Burgel U, Klingberg T, Larsson J, Zilles K,
916 Roland PE (1996) Two different areas within the primary motor cortex of man. Nature 382:805–807.
917 Geyer S, Matelli M, Luppino G, Zilles K (2000) Functional neuroanatomy of the primate isocortical motor
918 system. Anat Embryol (Berl) 202:443–474.
919 Glasser MF, Coalson TS, Robinson EC, Hacker CD, Harwell J, Yacoub E, Ugurbil K, Andersson J,
920 Beckmann CF, Jenkinson M, Smith SM, Van Essen DC (2016) A multi-modal parcellation of human
921 cerebral cortex. Nature 536:171–178.
922 Glasser MF, van Essen DC (2011) Mapping human cortical areas in vivo based on myelin content as
923 revealed by T1- and T2-weighted MRI. J Neurosci 31:11597–11616.
924 Groppa S, Oliviero A, Eisen A, Quartarone A, Cohen LG, Mall V, Kaelin-Lang A, Mima T, Rossi S,
925 Thickbroom GW, Rossini PM, Ziemann U, Valls-Solé J, Siebner HR (2012) A practical guide to

926 diagnostic transcranial magnetic stimulation: Report of an IFCN committee. Clin Neurophysiol
927 123:858–882.
928 Hagler DJ, Saygin AP, Sereno MI (2006) Smoothing and cluster thresholding for cortical surface-based
929 group analysis of fMRI data. Neuroimage 33:1093–1103.
930 Hamada M, Murase N, Hasan A, Balaratnam M, Rothwell JC (2013) The role of interneuron networks in
931 driving human motor cortical plasticity. Cereb Cortex 23:1593–1605.
932 Hardwick RM, Lesage E, Eickhoff CR, Clos M, Fox P, Eickhoff SB (2015) Multimodal connectivity of
933 motor learning-related dorsal premotor cortex. Neuroimage 123:114–128.
934 Helms G, Dathe H, Dechent P (2008) Quantitative FLASH MRI at 3T using a rational approximation of the
935 Ernst equation. Magn Reson Med 59:667–672.
936 Huntenburg JM, Bazin PL, Goulas A, Tardif CL, Villringer A, Margulies DS (2017) A Systematic
937 Relationship Between Functional Connectivity and Intracortical Myelin in the Human Cerebral Cortex.
938 Cereb Cortex 27:981–997.
939 Jäncke L, Loose R, Lutz K, Specht K, Shah NJ (2000) Cortical activations during paced finger-tapping
940 applying visual and auditory pacing stimuli. Cogn Brain Res 10:51–66.
941 Kammer T, Beck S, Erb M, Grodd W (2001) The influence of current direction on phosphene thresholds
942 evoked by transcranial magnetic stimulation. Clin Neurophysiol 112:2015–2021.
943 Kim SG, Knösche TR (2016) Intracortical myelination in musicians with absolute pitch: Quantitative
944 morphometry using 7-T MRI. Hum Brain Mapp 37:3486–3501.
945 Kuehn E, Dinse J, Jakobsen E, Long X, Schäfer A, Bazin PL, Villringer A, Sereno MI, Margulies DS (2017)
946 Body Topography Parcellates Human Sensory and Motor Cortex. Cereb Cortex 27:3790–3805.
947 Lang N, Harms J, Weyh T, Lemon RN, Paulus W, Rothwell JC, Siebner HR (2006) Stimulus intensity and
948 coil characteristics influence the efficacy of rTMS to suppress cortical excitability. Clin Neurophysiol
949 117:2292–2301.
950 Lemon R (2019) Recent advances in our understanding of the primate corticospinal system. F1000Research
951 8:F1000 Faculty Rev-274.
952 Lemon RN (2008) Descending Pathways in Motor Control. Annu Rev Neurosci 31:195–218.
953 Liewald D, Miller R, Logothetis N, Wagner HJ, Schüz A (2014) Distribution of axon diameters in cortical

white matter: an electron-microscopic study on three human brains and a macaque. Biol Cybern 108:541–557.

López-Alonso V, Cheeran B, Río-Rodríguez D, Fernández-Del-Olmo M (2014) Inter-individual variability in response to non-invasive brain stimulation paradigms. Brain Stimul 7:372–380.

Lutti A, Dick F, Sereno MI, Weiskopf N (2014) Using high-resolution quantitative mapping of R1 as an index of cortical myelination. Neuroimage 93:176–188.

Lutti A, Hutton C, Finsterbusch J, Helms G, Weiskopf N (2010) Optimization and validation of methods for mapping of the radiofrequency transmit field at 3T. Magn Reson Med 64:229–238.

Maertens De Noordhout A, Rapisarda G, Bogacz D, Gérard P, De Pasqua V, Pennisi G, Delwaide PJ (1999) Corticomotoneuronal synaptic connections in normal man. An electrophysiological study. Brain 122:1327–1340.

Nieuwenhuys R (2013) The myeloarchitectonic studies on the human cerebral cortex of the Vogt-Vogt school, and their significance for the interpretation of functional neuroimaging data. Brain Struct Funct 218:303–352.

Oldfield RC (1971) The assessment and analysis of handedness: The Edinburgh inventory. Neuropsychologia 9:97–113.

Opitz A, Windhoff M, Heidemann RM, Turner R, Thielscher A (2011) How the brain tissue shapes the electric field induced by transcranial magnetic stimulation. Neuroimage 58:849–859.

Pajevic S, Basser PJ, Fields RD (2014) Role of myelin plasticity in oscillations and synchrony of neuronal activity. Neuroscience 276:135–147.

Palmer E, Ashby P (1992) Corticospinal projections to upper limb motoneurones in humans. J Physiol 448:397–412.

Pascual-Leone A, Grafman J, Hallett M (1994) Modulation of cortical motor output maps during development of implicit and explicit knowledge. Science (80-) 263:1287–1289.

Peirce JW (2009) Generating stimuli for neuroscience using PsychoPy. Front Neuroinform 2:1–8.

Peterchev A V., Goetz SM, Westin GG, Luber B, Lisanby SH (2013) Pulse width dependence of motor threshold and input-output curve characterized with controllable pulse parameter transcranial magnetic stimulation. Clin Neurophysiol 124:1364–72.

982 Picard N, Strick PL (2001) Imaging the premotor areas. Curr Opin Neurobiol 11:663–672.
983 Pienaar R, Fischl B, Caviness V, Makris N, Grant PE (2008) A methodology for analyzing curvature in the
984 developing brain from preterm to adult. Int J Imaging Syst Technol 18:42–68.
985 Raffin E, Pellegrino G, Di Lazzaro V, Thielscher A, Siebner HR (2015) Bringing transcranial mapping into
986 shape: Sulcus-aligned mapping captures motor somatotopy in human primary motor hand area.
987 Neuroimage 120:164–175.
988 Raffin E, Siebner HR (2018) Use-Dependent Plasticity in Human Primary Motor Hand Area: Synergistic
989 Interplay Between Training and Immobilization. Cereb Cortex 29:356–371.
990 Rathelot J-A, Strick PL (2006) Muscle representation in the macaque motor cortex: An anatomical
991 perspective. Proc Natl Acad Sci 103:8257–8262.
992 Rathelot J-A, Strick PL (2009) Subdivisions of primary motor cortex based on cortico-motoneuronal cells.
993 Proc Natl Acad Sci 106:918–923.
994 Rossi S et al. (2009) Safety, ethical considerations, and application guidelines for the use of transcranial
995 magnetic stimulation in clinical practice and research. Clin Neurophysiol 120:2008–2039.
996 Rossini PM et al. (2015) Non-invasive electrical and magnetic stimulation of the brain, spinal cord, roots and
997 peripheral nerves: Basic principles and procedures for routine clinical and research application: An
998 updated report from an I.F.C.N. Committee. Clin Neurophysiol 126:1071–1107.
999 Salvador R, Silva S, Basser PJ, Miranda PC (2011) Determining which mechanisms lead to activation in the
1000 motor cortex: A modeling study of transcranial magnetic stimulation using realistic stimulus
1001 waveforms and sulcal geometry. Clin Neurophysiol 122:748–758.
1002 Sánchez-Panchuelo RM, Francis ST, Schluppeck D, Bowtell RW (2012) Correspondence of human visual
1003 areas identified using functional and anatomical MRI in vivo at 7 T. J Magn Reson Imaging 35:287–
1004 299.
1005 Sarfeld AS, Diekhoff S, Wang LE, Liuzzi G, Uludağ K, Eickhoff SB, Fink GR, Grefkes C (2012)
1006 Convergence of human brain mapping tools: Neuronavigated TMS Parameters and fMRI activity in the
1007 hand motor area. Hum Brain Mapp 33:1107–1123.
1008 Seidl AH, Rubel EW, Harris DM (2010) Mechanisms for adjusting interaural time differences to achieve
1009 binaural coincidence detection. J Neurosci 30:70–80.

1010 Sereno MI, Lutti A, Weiskopf N, Dick F (2013) Mapping the Human Cortical Surface by Combining
1011 Quantitative T1 with Retinotopy†. Cereb Cortex 23:2261–2268.
1012 Shams Z, Norris DG, Marques JP (2019) A comparison of in vivo MRI based cortical myelin mapping using
1013 T1w/T2w and R1 mapping at 3T. PLoS One 14:e0218089.
1014 Siebner HR (2020) Does TMS of the precentral motor hand knob primarily stimulate the dorsal premotor
1015 cortex or the primary motor hand area? Brain Stimul 13:517–551.
1016 Smith S, Jenkinson M, Woolrich MW, Saunders J, Brady JM, Matthews PM, Drobnjak I, Behrens TEJ, De
1017 Stefano N, Jenkinson M, Bannister PR, Flitney DE, Beckmann CF, Zhang Y, Niazy RK, Johansen-
1018 Berg H, Smith SM, Vickers J, De Luca M (2004) Advances in functional and structural MR image
1019 analysis and implementation as FSL. Neuroimage 23 Suppl 1:S208-19.
1020 Sugiura M, Kawashima R, Takahashi T, Xiao R, Tsukiura T, Sato K, Kawano K, Iijima T, Fukuda H (2001)
1021 Different distribution of the activated areas in the dorsal premotor cortex during visual and auditory
1022 reaction-time tasks. Neuroimage 14:1168–1174.
1023 Teitti S, Määttä S, Säisänen L, Könönen M, Vanninen R, Hannula H, Mervaala E, Karhu J (2008) Non-
1024 primary motor areas in the human frontal lobe are connected directly to hand muscles. Neuroimage
1025 40:1243–1250.
1026 Thielscher A, Antunes A, Saturnino GB (2015) Field modeling for transcranial magnetic stimulation: A
1027 useful tool to understand the physiological effects of TMS? In: Proceedings of the Annual International
1028 Conference of the IEEE Engineering in Medicine and Biology Society, EMBS, pp 222–225.
1029 Thielscher A, Kammer T (2004) Electric field properties of two commercial figure-8 coils in TMS:
1030 Calculation of focality and efficiency. Clin Neurophysiol 115:1697–1708.
1031 Thielscher A, Opitz A, Windhoff M (2011) Impact of the gyral geometry on the electric field induced by
1032 transcranial magnetic stimulation. Neuroimage 54:234–243.
1033 Timmler S, Simons M (2019) Grey matter myelination. Glia 67:2063–2070.
1034 Vaalto S, Julkunen P, Säïsänen L, Könönen M, Määttä S, Karhu J (2016) Increased Inhibition in Non-
1035 Primary Motor Areas of String-Instrument Players: A Preliminary Study with Paired-Pulse Transcranial
1036 Magnetic Stimulation. Brain Plast 1:223–234.
1037 Vaalto S, Säisänen L, Könönen M, Julkunen P, Hukkanen T, Määttä S, Karhu J (2011) Corticospinal output

and cortical excitation-inhibition balance in distal hand muscle representations in nonprimary motor area. Hum Brain Mapp 32:1692–1703.

Veldema J, Bösl K, Nowak DA (2017) Motor Recovery of the Affected Hand in Subacute Stroke Correlates with Changes of Contralesional Cortical Hand Motor Representation. Neural Plast 2017:6171903.

Volz LJ, Hamada M, Rothwell JC, Grefkes C (2015) What Makes the Muscle Twitch: Motor System Connectivity and TMS-Induced Activity. Cereb Cortex 25:2346–2353.

Ward NS, Bestmann S, Hartwigsen G, Weiss MM, Christensen LOD, Frackowiak RSJ, Rothwell JC, Siebner HR (2010) Low-Frequency Transcranial Magnetic Stimulation over Left Dorsal Premotor Cortex Improves the Dynamic Control of Visuospatially Cued Actions. J Neurosci 30:9216–9223.

Wassermann EM, Pascual-Leone A, Valls-Solé J, Toro C, Cohen LG, Hallett M (1993) Topography of the inhibitory and excitatory responses to transcranial magnetic stimulation in a hand muscle. Electroencephalogr Clin Neurophysiol Evoked Potentials 89:424–433.

Weise K, Numssen O, Thielscher A, Hartwigsen G, Kn TR (2020) A novel approach to localize cortical TMS effects. Neuroimage 209:116486.

Weiskopf N, Helms G (2008) Multi-parameter mapping of the human brain at 1mm resolution in less than 20 minutes N. In: Proceedings of the 16th Scientific Meeting ISMRM.

Weiskopf N, Lutti A, Helms G, Novak M, Ashburner J, Hutton C (2011) Unified segmentation based correction of R1 brain maps for RF transmit field inhomogeneities (UNICORT). Neuroimage 54:2116–2124.

West DC, Wolstencroft JH (1983) Strength-duration characteristics of myelinated and non-myelinated bulbospinal axons in the cat spinal cord. J Physiol 337:37–50.

Witham CL, Fisher KM, Edgley SA, Baker SN (2016) Corticospinal inputs to primate motoneurons innervating the forelimb from two divisions of primary motor cortex and area 3a. J Neurosci 36:2605–2616.

Witt ST, Laird AR, Meyerand ME (2008) Functional neuroimaging correlates of finger-tapping task variations: An ALE meta-analysis. Neuroimage 42:343–356.

Worsley KJ, Marrett S, Neelin P, Vandal AC, Friston KJ, Evans AC (1996) A unified statistical approach for determining significant signals in images of cerebral activation. Hum Brain Mapp 4:58–73.

Yousry TA, Schmid UD, Alkadhi H, Schmidt D, Peraud A, Buettner A, Winkler P (1997) Localization of the motor hand area to a knob on the precentral gyrus. A new landmark. Brain 120:141–157.

Ziemann U, Siebner HR (2015) Inter-subject and intersession variability of plasticity induction by non-invasive brain stimulation: Boon or bane? Brain Stimul 8:662–663.

Figure Legends

Figure 1

Multimodal mapping of the precentral hand knob.

(A) The top panel illustrates sulcus-aligned mapping with single-pulse transcranial magnetic stimulation (TMS). The mapping grid consists of five lines with seven target sites per line. The lines follow the individual shape of the precentral gyrus forming the right precentral hand knob. Single-pulse TMS was applied at each target site and motor evoked potentials (MEPs) were recorded from left first dorsal

interosseous (FDI) and abductor digiti minimi (ADM) muscles. The first two lines (light blue) corresponded to posterior lip of the pre-Central Gyrus crown (Pre-CG). The remaining three lines (orange) corresponded to the top of the Pre-CG crown till the pre-Central Sulcus (Pre-CS). The bottom panel shows colour-coded corticomotor maps for the FDI and ADM muscle. Each square represents a stimulation site and the colour codes the mean MEP amplitude. Note that the FDI muscle is represented more laterally respect to the ADM muscle. B) Surface-rendered group map of the simulated electric field strength induced by TMS. (C) Structural MRI: Average distribution of cortical thickness (top) and cortical myelination (bottom) measured as longitudinal relaxation rate R1= 1/T1 across all subjects. (D) Average fMRI activity for voluntary abduction-adduction movements of the left index (FDI) and little (ADM) fingers during a visually cued motor task at 1 Hz.

Figure 2

Structural, functional and electrical field properties of the right precentral gyrus (Pre-CG).

(A) The left panel represents the right precentral Region of Interest (ROI) considered for the analyses, namely the light blue mask including the gyral wall facing the Central Sulcus (CS), caudal pre-CG ROI, and the orange mask composed of the gyral crown and gyral wall facing the pre-Central Sulcus (pre-CS), rostral pre-CG ROI. Bottom figure indicates the cross section (following the blue dotted line) of Pre-CG with a schematic representation of caudal pre-CG and rostral pre-CG ROIs. (B-E) Significant differences are evident between the caudal pre-CG and rostral pre-CG ROIs regarding the cortical myelin content (B), functional activation during the visually cued movement repetition task (C), mean cortical thickness (D) and mean TMS-induced field strength (E). Each panel consists of a bar-plot representing the regional mean (left) and a surface-rendered voxel-wise group map, including the borders of the two ROIs.

Figure 3

Corticomotor maps of the right precentral hand knob derived from sulcus-shape based TMS mapping.

(A) Two-dimensional colour-coded map illustrating the spatially distribution of corticomotor excitability in the right precentral hand knob. The motor hotspot is indicated by an “X”. The left panel shows the map of

an individual (subject n. 3) with caudal hotspot location in the posterior lip of the precentral gyrus for the FDI muscle (upper panel) and ADM muscle (lower panel). The right panel shows the map of an individual (subject n. 18) with a more rostral hot spot at the top of the precentral crown. Each square corresponds to a specific target site determined by its medio-lateral (target 1 to 7) and posterior-anterior position (lines 1-5). (B) Scatter plots plotting the x (medio-lateral direction) or y (posterior-anterior direction) coordinates of the motor hot spot in MNI space against the shortest MEP latency recorded at the motor hot spot location. Significant correlations with MEPs latencies were only found for the posterior-anterior position of the hotspot coordinates (y-coordinates) but not for medio-lateral psoition (x-coordinates). Open black circles indicate participants with a more caudal hot spot location in the posterior lip of Pre-CG (located on lines 1 and 2 of the mapping grid). Close black circles indicate participants with a more rostral hot spot location at the top of the Pre-CG crown (located on line 3 or 4 of the mapping grid). Please, note that the labelling of the x-axes is identical for all four scatter plots.

Figure 4

A higher cortical myelin content in right precentral motor hand knob is associated with a more rostral hot-spot location

Positive linear relationship between cortical myelination (as indexed by the mean R1 signal) in the precentral hand knob and the spatiotemporal rostrality index of the TMS hot-spot for the FDI (A) and ADM muscle (C). Open and close black circles indicate subjects with hotspot located in the posterior lip of precentral crown and top of the precentral crown, respectively.

Surface-rendered statistical parametric maps: The maps show voxels with a significant positive relationship between the precentral myelin-related signal and rostrality index for FDI (B) and ADM hot spot (D).

Pre-CG: Pre-Central Gyrus; ROI: Region of interest, FDI: first dorsal interosseous; ADM= abductor digiti minimi.

Figure 5

A higher cortical myelin content in right precentral motor hand knob is associated with a higher functional activation during visually cued repetitive finger movements

Positive linear relationship between cortical myelination (as indexed by the mean R1 signal) in the precentral hand knob and the BOLD signal increase during the visuo-motor abduction task. The same positive relationship became evident when the task was performed with the left index finger (A) or little finger (C). Open and close black circles indicate subjects with hotspot located in the posterior lip of precentral crown and top of the precentral crown, respectively. Surface-rendered statistical parametric maps: The maps show voxels with a significant positive relationship between the precentral myelin-related signal and the task-related BOLD increase for index (B) and little finger (D). Pre-CG: Pre-Central Gyrus; ROI: Region of interest.

Figure 6

Relationship between the cortical myelin content in right precentral motor hand knob and temporal synchronization of repetitive finger movements.

Negative linear relationship between cortical myelination (as indexed by the mean R1 signal) in the precentral hand knob and the coefficient of variation of the inter-movement interval during the visuo-motor abduction task. The same negative relationship became evident when the task was performed with the left index finger (A) or little finger (C). Open and close black circles indicate subjects with hotspot located in the posterior lip of precentral crown and top of the precentral crown, respectively. Surface-rendered voxel-wise correlation maps indicating a negative relationship between precentral cortical myelination and the coefficient of variation of the inter-movement interval during the visuo-motor abduction task and for the index (B) and little finger (D). Statistical maps are thresholded at $p_{uncorr}<0.01$ for illustrative purposes. Pre-CG: Pre-Central Gyrus; ROI: Region of interest.

Figure 7

Simulations of the electric field strength induced by TMS at motor hotspot location.

Colour-coded surface-rendered group maps for participants with preferential hotspot location in the posterior lip of the precentral gyrus (A) or at the top of the precentral crown (B). The surface-based statistical map (C) shows a single cluster in the posterior lip of the precentral gyrus where participants with preferential hotspot location in the posterior lip of the Pre-Central Gyrus crown display a higher electrical

field strength than participants with a more rostral location of motor hotspot. Between-groups difference of the mean electric field strength extracted from the significant cluster in the posterior lip region (D) . Mean electrical field strength in this cluster is higher in subjects with a more posterior motor hotspot location in the precentral crown (white column) than in subjects with a more rostral motor hotspot location (black bar), * $t_{(16.7)}= 2.604, p= 0.019$; unpaired t-test.

Table 1

The table lists demographic and electrophysiological data (mean±SEM)

RMT = Resting motor threshold; %MSO= percentage of maximum stimulation output; MEP = Motor evoked potential; FDI= first dorsal interosseous; ADM= abductor digiti minimi. The p-values refer to between-group comparisons comparing mean values of variables (Caudal hotspot group vs Rostral hotspot group).

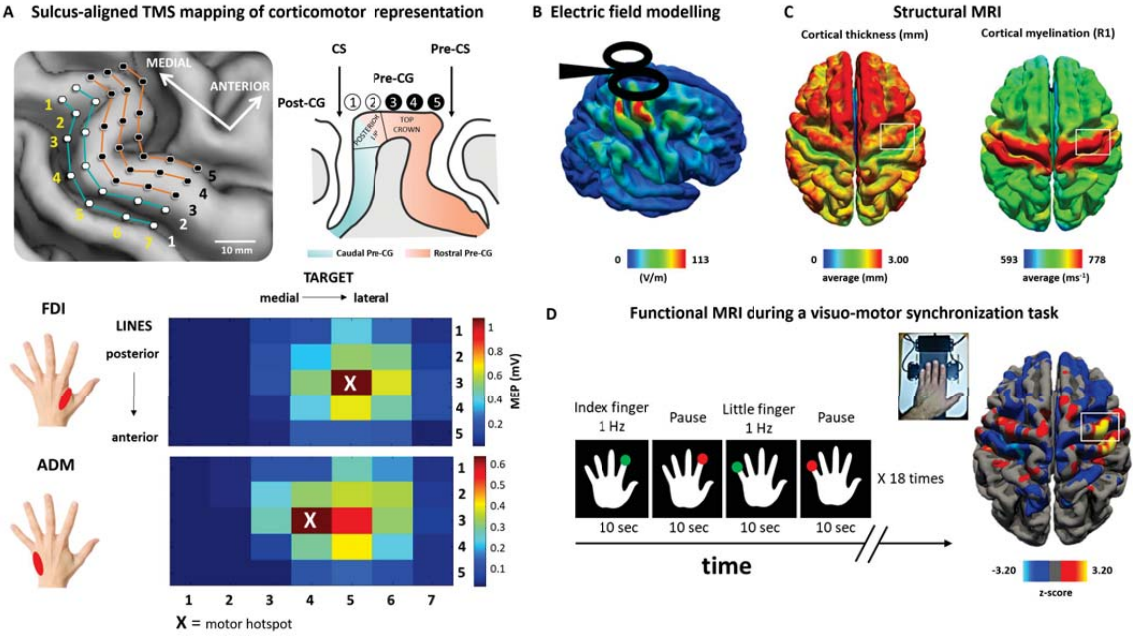

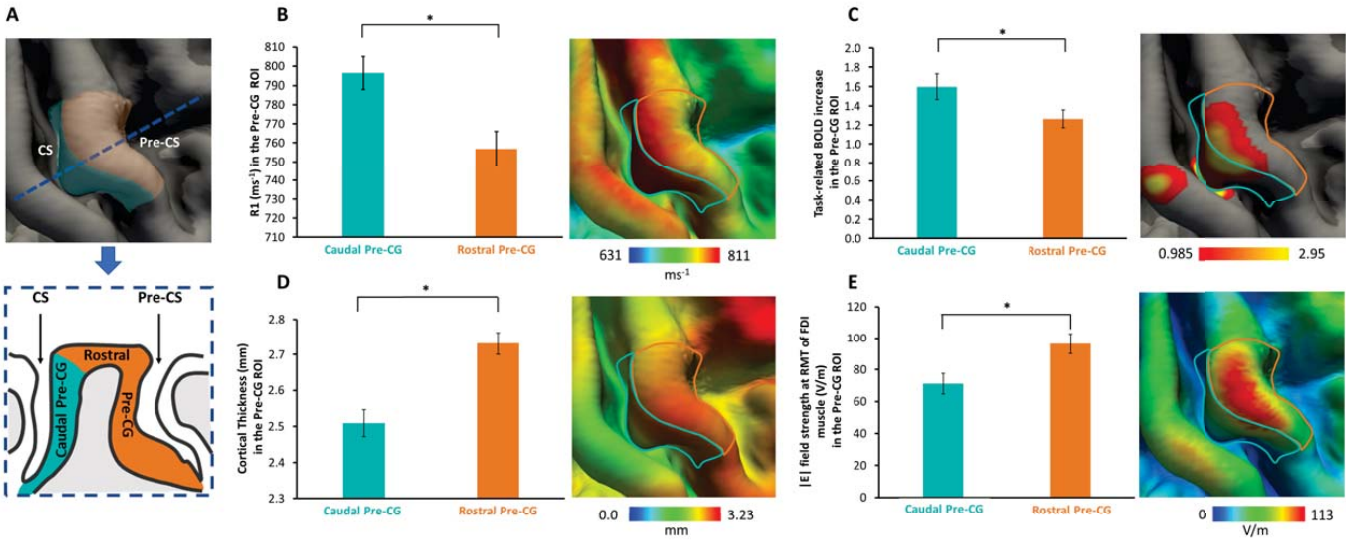

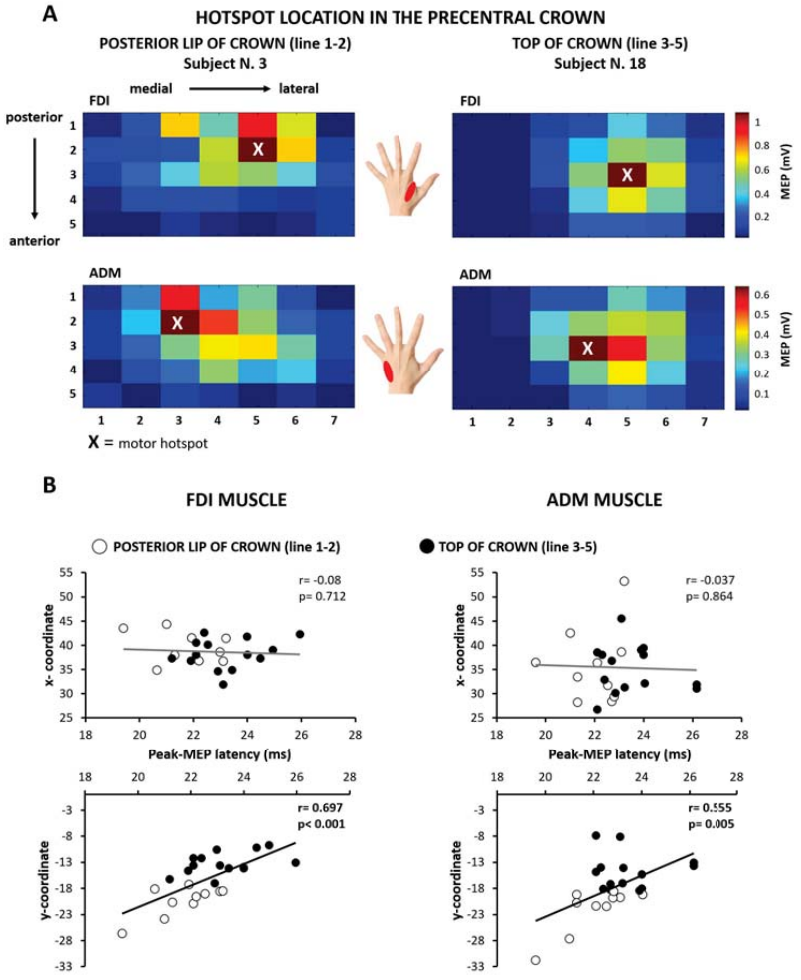

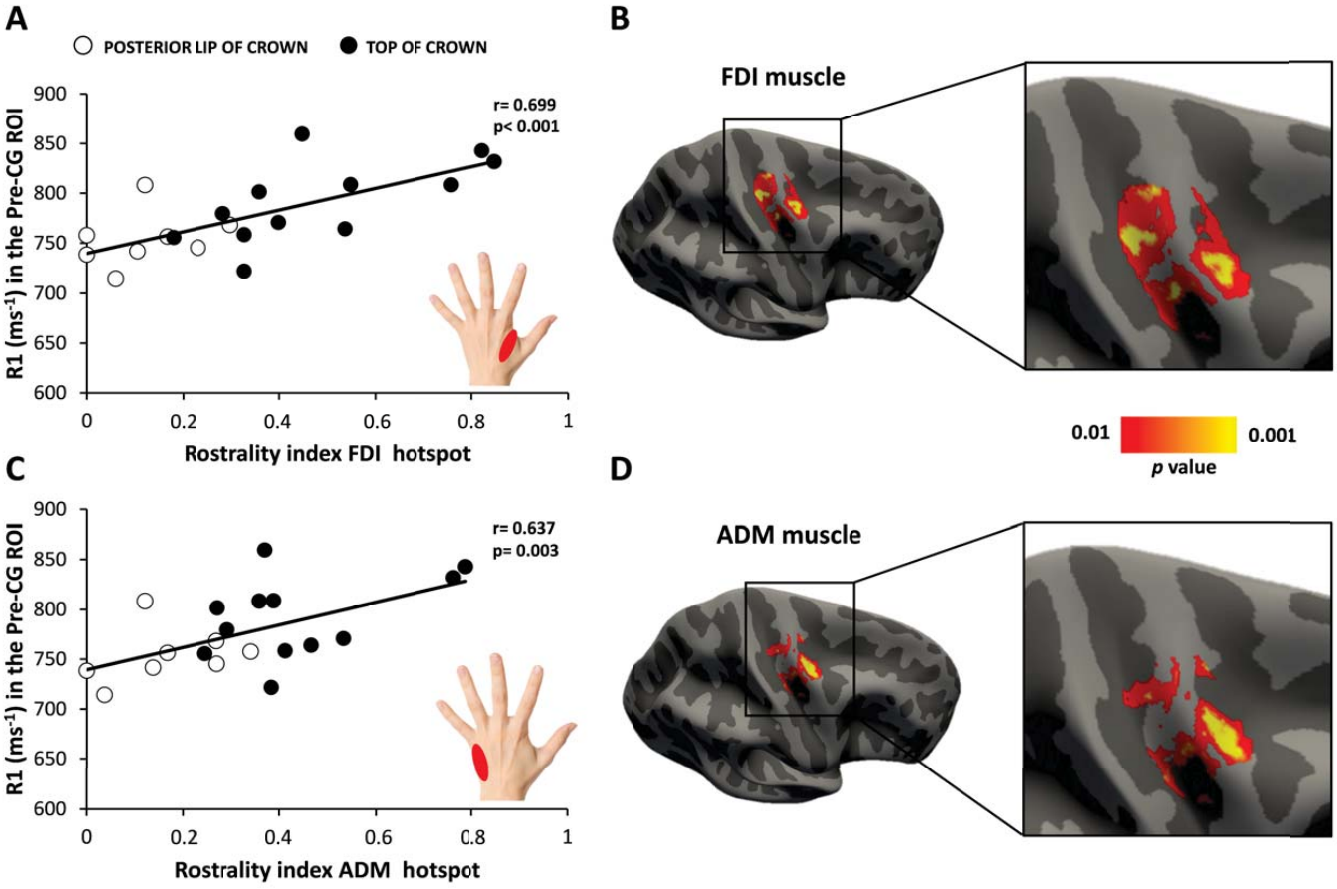

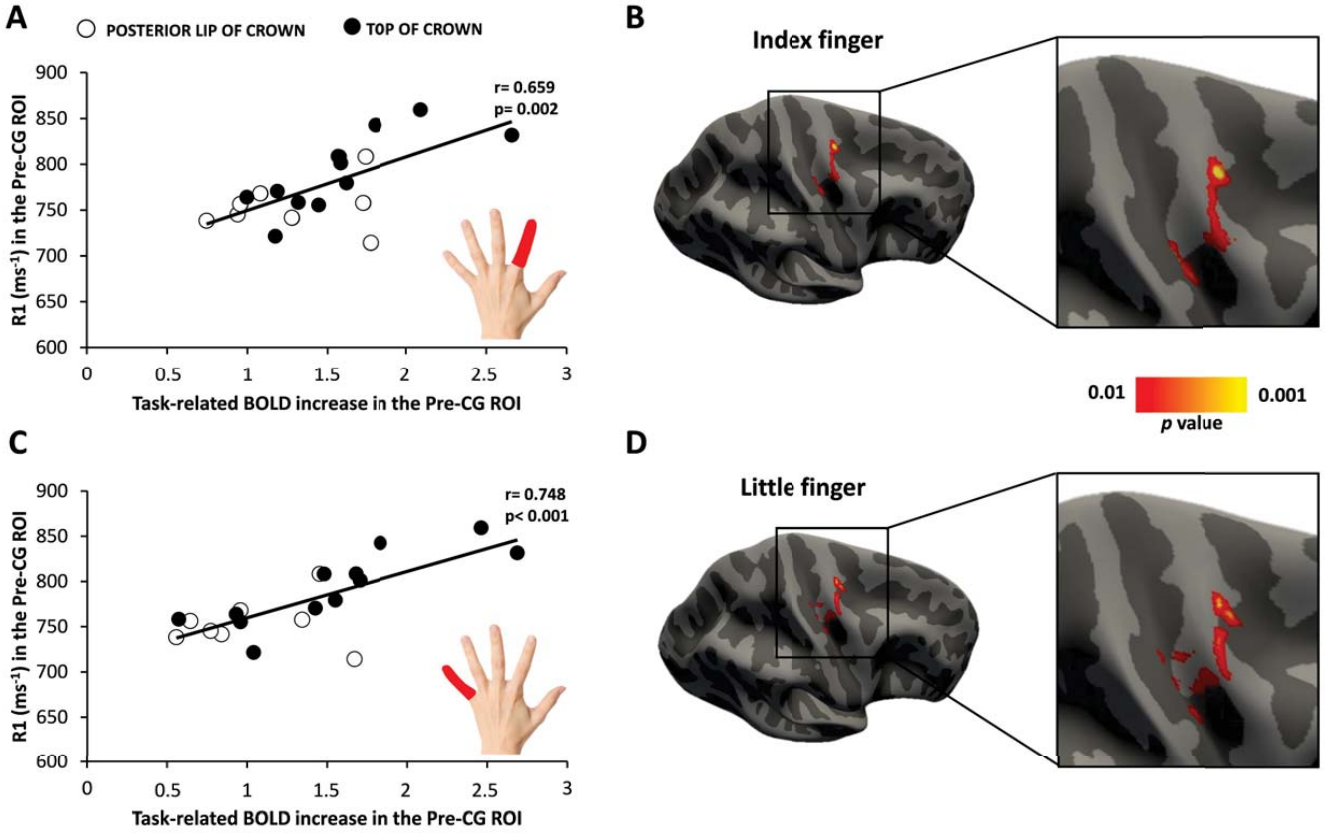

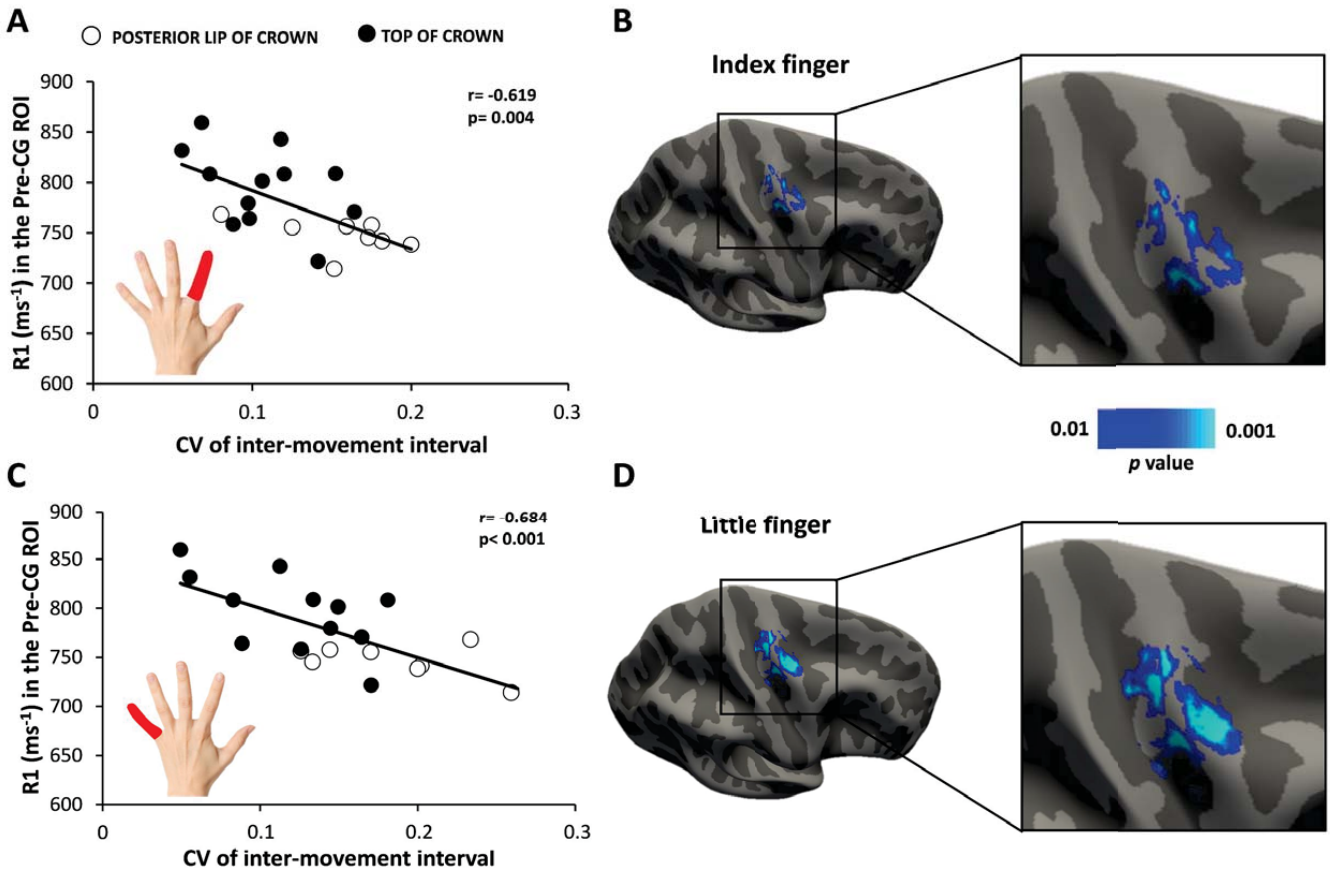

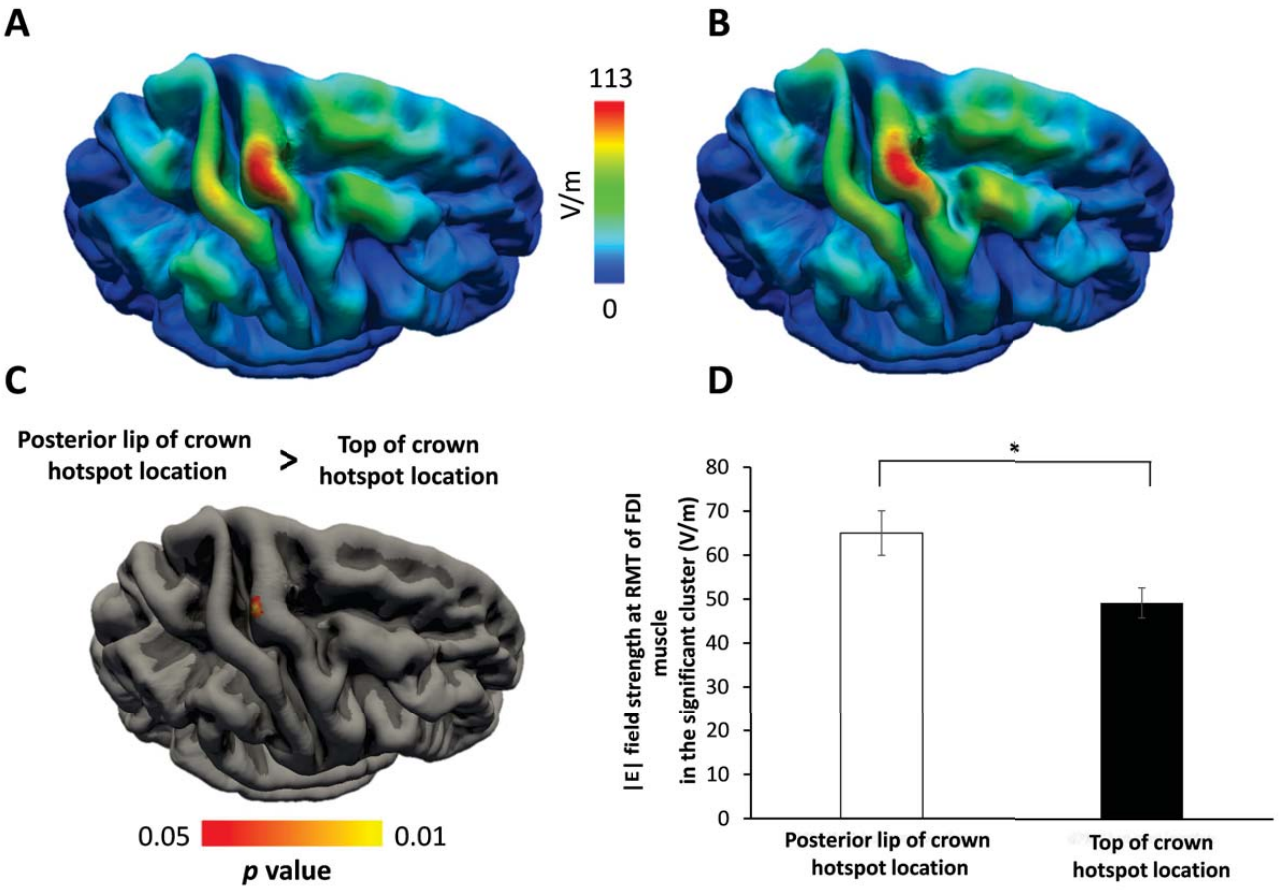

	All participants (n=24)	Caudal hotspot group (n=10)	Rostral hotspot group (n=14)	*Statistic*, p-value
Sex (Male/Female)	12/12	5/5	7/7	χ^2= 0, p=1
Age (Years)	24.2 ± 0.9	22.6 ± 1.1	25.4 ± 1.3	$t_{(22)}$= -1.699, p= 0.11
Height (cm)	172.9 ± 6.0	171.5 ± 4.7	173.9 ± 6.8	$t_{(22)}$= -1.004, p= 0.326
RMT of FDI muscle (% MSO)	58.1 ± 2.2	55.3 ± 2.4	60.1 ± 3.4	$t_{(21.6)}$= -1.144, p= 0.27
MEP latency at hotspot (ms)				
Left FDI muscle	22.6 ± 0.3	21.7 ± 0.4	23.3 ± 0.4	$t_{(20.9)}$= -2.952, p= 0.008
Left ADM muscle	22.9 ± 0.3	22.0 ± 0.4	23.5 ± 0.4	$t_{(21.1)}$= -3.033, p= 0.006
MEP Amplitude at hotspot (mV)				
Left FDI muscle	1.1 ± 0.2	1.3 ± 0.3	1.0 ± 0.2	$t_{(14.46)}$= 0.804, p= 0.43
Left ADM muscle	0.5 ± 0.1	0.4 ± 0.1	0.6 ± 0.1	$t_{(21.6)}$= -0.682, p= 0.5
MNI-coordinates of motor hotspot				
Left FDI muscle (x-coordinate)	38.7 ± 0.6	39.4 ± 1.0	38.1 ± 0.8	$t_{(19.1)}$= 1.02, p= 0.32
Left FDI muscle (y-coordinate)	-16.6 ± 1.0	-21.3 ± 1.2	-13.2 ± 0.6	$t_{(13)}$= -6.11, p= <0.001
Left FDI muscle (z-coordinate)	66.5 ± 0.6	65.2 ± 0.9	67.4 ± 0.7	$t_{(16)}$= -1.873, p= 0.08
Left ADM muscle (x-coordinate)	35.4 ± 1.2	35.8 ± 2.4	35.1 ± 1.3	$t_{(14.35)}$= 0.269, p= 0.79
Left ADM muscle (y-coordinate)	-17.8 ± 1.1	-21.7 ± 1.4	-15.0 ± 1.0	$t_{(16.7)}$= -3.85, p= 0.001
Left ADM muscle (z-coordinate)	69.1 ± 1.0	67.8 ± 1.6	70.1 ± 1.3	$t_{(18.8)}$= -1.113, p= 0.28
Spatiotemporal rostrality index				
Left FDI muscle	0.34 ± 0.05	0.14 ± 0.03	0.49 ± 0.05	$t_{(15.6)}$= -6.568, p <0.001
Left ADM muscle	0.32 ± 0.04	0.18 ± 0.03	0.42 ± 0.05	$t_{(16.7)}$= -3.850, p <0.001

Table 1.

The table lists demographic and electrophysiological data (mean±SEM)

RMT = Resting motor threshold; %MSO= percentage of maximum stimulation output; MEP = Motor evoked potential; FDI= first dorsal interosseous; ADM= abductor digiti minimi. The p-values refer to between-group comparisons comparing mean values of variables (Caudal hotspot group vs Rostral hotspot group).